Surface Modes of Vibration and Optical Properties of an Ionic-Crystal Slab*

W. E. Jones† and Ronald Fuchs
Institute for Atomic Research and Department of Physics, Iowa State University, Ames, Iowa 50010
(Received 26 April 1971)

A formalism is developed for calculating the normal modes of vibration of an ionic-crystal slab having the NaCl structure. The slab consists of a finite number of (100) planes oriented normal to the z axis and is of infinite extent in the x and y directions. The derivation of the dynamical matrix takes into account the free surfaces of the slab as well as the effect of retardation of the Coulomb interaction. Retardation is easily excluded from the theory by letting the speed of light c become infinite in the Coulomb contributions to the dynamical matrix. The unretarded normal-mode frequencies and eigenvectors are calculated for a seven-layer slab for values of the wave vector chosen along the x axis and ranging from zero out to the boundary of the two-dimensional first Brillouin zone. The properties of the optical surface modes are discussed in detail. If an electromagnetic wave is incident upon the slab, the optical properties of the slab can be found by calculating the total electric field which exists in the regions of space on either side of the slab as a superposition of the incident field and the induced field arising from the ionic motion within the slab. For both P and S polarizations of the incident field, peaks in the infrared absorption are found to occur at frequencies corresponding to certain optical modes of the slab. The calculated results offer a qualitative explanation of the transmittance of a thin LiF film as experimentally observed by Berreman.

I. INTRODUCTION

In recent years there have been several theoretical investigations of the normal modes of vibration of a point-ion model of an ionic-crystal slab of finite thickness and extending to infinity in the two lateral directions.[1-6] Because of the translational symmetry in directions parallel to the plane of the slab, one assumes normal modes in which the ionic displacement amplitudes are wavelike in these directions. The problem is then to determine both how the frequencies ω of these normal modes depend on the two-dimensional wave vector $\vec{q}$ in the plane of the slab and how the ionic displacement amplitudes vary in the direction perpendicular to the slab for each normal mode.

Investigations of the normal modes have been carried out both excluding and including the retardation of the Coulomb interaction. Inclusion of retardation significantly affects only the long-wavelength optical modes. Those theories which exclude retardation will be discussed first.

The unretarded normal modes of the slab can be classified as either bulk modes or surface modes. Bulk modes are ones in which the variation of the ionic displacement amplitudes in the direction perpendicular to the slab is wavelike in character. Surface modes are ones in which the ionic displacement amplitudes decrease with increasing distance into the slab from the surfaces, i.e., they are localized at the surfaces. Both bulk modes and surface modes can also be categorized as acoustical or optical in the usual manner and as transverse or longitudinal depending upon the direction of the ionic displacements at $\vec{q}=0$. Modes for which the ionic motion is parallel to the slab at $\vec{q}=0$ are transverse modes; if the motion is normal to the plane of the slab, then the modes are longitudinal.

Fuchs and Kliewer[1] determined the properties of the optical modes of vibration of an ionic-crystal slab of the NaCl type in the long-wavelength approximation by introducing a macroscopic polarization and an average electric field as slowly varying functions of position within the slab. Using this approximation, and neglecting any changes in the short-range forces acting on surface ions, the equation of motion of a pair of ions leads to a set of integral equations which yield the properties of the optical modes. Choosing their z axis normal to the plane of the slab and taking $q_y=0$, they found the optical bulk modes of the slab to exist at the usual transverse-optical and longitudinal-optical frequencies, ω_{TO} and ω_{LO}, of the infinitely extended crystal. Moreover, they found two optical surface modes in which the ionic displacement amplitudes decreased exponentially with increasing distance into the slab from the surfaces. The frequencies of these surface modes are at ω_{TO} and ω_{LO} when $q_x=0$, the lower mode being transverse and the upper mode longitudinal. As q_x increases, they start to move together and approach a frequency between ω_{TO} and ω_{LO}. Also, these modes are such that the ionic displacement amplitudes are constant for $q_x=0$; i.e., the surface modes cease to be localized at the surfaces in the $\vec{q}=0$ limit.

Lucas[2] has examined the normal modes of a slab for $\vec{q}=0$ in a calculation which included changes in the short-range forces acting on surface ions. For a slab of N layers of ions, his calculation reduced to a study of two coupled parallel diatomic chains,

each having N ions. All transverse modes of the chain will then be doubly degenerate modes of the slab because of the symmetry of the x and y directions in the plane of the slab. By first solving this double chain problem for $N=\infty$ and then applying appropriate boundary conditions for the case of finite N, he found two nearly degenerate transverse-optical (TO) surface modes with frequencies slightly below ω_{TO}. These are modes in which the ionic displacements are of even and odd parity with respect to the center of the slab. His results differ from those of Fuchs and Kliewer[1] in that he found two transverse surface modes near ω_{TO}, rather than one; moreover, both of the modes are localized at the surface for $\vec{q}=0$.

More recently, Tong and Maradudin[3] have calculated the normal modes of a point-ion model of a NaCl slab bounded by a pair of (110) faces normal to the z direction. Their solution uses lattice-dynamics techniques including corrections to the forces acting on surface ions and requires the diagonalization of a $6N\times 6N$ (N = number of layers of ions in the slab) matrix for values of $\vec{q}$ throughout the two-dimensional first Brillouin zone. They performed this calculation and reported finding a total of six optical surface modes and two acoustical surface modes. At $\vec{q}=0$ they found two nearly degenerate TO surface modes, of even and odd parities, whose frequencies are slightly less than ω_{TO}. Each of these modes is doubly degenerate and localized at the surface for $\vec{q}=0$. This essentially agrees with the results found by Lucas. Going away from $\vec{q}=0$, they found two nearly degenerate optical surface modes at frequencies roughly midway between ω_{TO} and ω_{LO}. They found that these two modes have limiting frequencies at $\vec{q}=0$ well below ω_{LO} and are not localized at the surfaces at the point $\vec{q}=0$. None of these optical surface modes seem to exhibit the wave-vector dependence predicted by Fuchs and Kliewer.

Thus the results of Lucas agree with those of Tong and Maradudin at the point $\vec{q}=0$ and the results of Fuchs and Kliewer seem to disagree both with Lucas and with Tong and Maradudin. Lucas explained the discrepancy between his results and those of Fuchs and Kliewer as being due to their neglect of the modifications of the forces acting on the surface ions. Tong and Maradudin stated that Fuchs and Kliewer made an invalid long-wavelength approximation by converting two-dimensional lattice sums of Coulomb forces between the ions into integrals. They also noted that Fuchs and Kliewer did not modify the forces on surface ions.

Chen, Allen, Alldredge, and de Wette[4] have studied the normal modes of vibration of a 15-layer NaCl slab, using the same model as that of Tong and Maradudin. They plot the dependence of the normal-mode frequencies on $\vec{q}$ in considerable detail for $\vec{q}$ values along selected paths in the two-dimensional Brillouin zone. Their results differ significantly from those of Tong and Maradudin; one pair of surface modes has a different behavior near $\vec{q}=0$, and at the edge of the Brillouin zone they find many surface modes existing in gaps between bands of bulk modes. In Sec. IX we shall discuss their results in more detail.

Kliewer and Fuchs[5] have also studied the effects of including retardation of the Coulomb interaction on the normal modes of an ionic-crystal slab. They found that these coupled phonon-photon modes of the slab fell into two classes: nonradiative modes with exponentially damped fields outside the slab, and radiative modes with incoming or outgoing waves outside the slab. The nonradiative modes exist for $q>\omega/c$, where c is the speed of light and q is the magnitude of $\vec{q}$, and were calculated using a technique very similar to that used for the unretarded modes. When retardation is included, the two optical surface modes were found to exist only for $q>\omega/c$. Both modes approach $\omega=\omega_{TO}$ as q approaches the line $q=\omega/c$. As q increases from ω_{TO}/c, the frequency of the high-frequency mode increases rapidly to a maximum below $\omega=\omega_{LO}$ and then gradually drops back down, whereas the frequency of the low-frequency mode increases monotonically. Both modes than approach a common frequency between ω_{TO} and ω_{LO}, as did the unretarded modes, when $q\gg\omega/c$.

In a recent paper, Bryksin and Firsov[6] have also derived expressions for both the unretarded and retarded dynamical matrices of an ionic-crystal slab. However, they did not make any actual calculations of the normal modes of a slab containing a specific number of layers of ions and did not present complete expressions for all elements of the dynamical matrix. In the long-wavelength limit their unretarded theory predicted the existence of 24 surface modes, apparently independent of the number of layers in the slab. These 24 modes were found to be of two distinct types. Twelve of them were such that the amplitudes of the ionic displacements decay gradually away from the surfaces of the slab and the other twelve were such that this decay of ionic displacements was much more rapid (approximately within a lattice constant). The modes of the former type were found to arise from the long-range Coulomb forces and correspond in behavior to those found by Fuchs and Kliewer.[1] The modes of the latter type are related to the short-range forces acting on ions on or near the surfaces. For $qa\geq 1$ the number of modes was found to drop to 12 since the two types apparently merge as the former type becomes strongly localized at the surfaces. They state that their theory provides a microscopic basis for the validity of the dielectric-constant formalism used by Fuchs and

Kliewer in their treatment of the surface modes arising from the long-range Coulomb forces both with and without retardation.

In this paper we examine the normal modes of vibration of an ionic-crystal slab to try to resolve some of the discrepancies noted between the results of the preceding theories. We first develop a theory from which the normal modes of the slab may be calculated including the effects of retardation. If we then let the speed of light c become infinite, the theory yields the unretarded normal modes. We calculate the unretarded modes of a seven-layer slab and discuss our results in relation to those previously mentioned.

We also develop a theory which allows us to calculate the infrared optical properties of an ionic-crystal slab from its unretarded normal-mode frequencies and eigenvectors. We calculate the transmittance, reflectance, and absorptance of a 15-layer slab with the radiation incident at an angle of 75°. The calculations are made for both P and S polarizations of the incident electric field. The results are discussed and compared with the results of two different studies by Tong and Maradudin[3] and Berreman.[7]

II. LATTICE DYNAMICS OF AN IONIC-CRYSTAL SLAB

We consider a diatomic ionic-crystal slab of finite thickness oriented normal to the z axis and extending to infinity in the x and y directions. We assume the crystal structure to be of the NaCl type and the z axis to be along the [001] direction so that the slab is made up of N planes of point ions having masses m_j and charges e_j where $j=1, 2$ denotes the two types of ions. Each plane of ions is then considered as a perfect two-dimensional lattice divided up into a network of unit cells, each having the same arrangement of ions. The sides of a unit cell are determined by two basis vectors $\vec{a}_1$ and $\vec{a}_2$ and the area of a unit cell is $|\vec{a}_1\times\vec{a}_2|$. The points at the corners of the unit cells form a Bravais lattice defined by the general lattice vectors $\vec{l}=l_1\vec{a}_1+l_2\vec{a}_2$, where l_1 and l_2 are integers which may be positive, negative, or zero. The equilibrium positions of the ions within a unit cell are specified by the vectors $\vec{s}_j$, measured from the reference corner of the cell. We approximate the equilibrium positions of the ions to be the same as in an infinite crystal.[8]

In order to simplify the derivation of the dynamical matrix in the following sections we choose the origin of coordinates at the equilibrium site of a positive ion on one of the surface layers of the slab as shown in Fig. 1. The x and y axes are chosen along ⟨110⟩ directions, and the planes of ions are seen to intersect the z axis at $l_z=l_3r_0$, where $l_3=0, 1, 2, \ldots, N-1$ and r_0 is the nearest-neighbor distance. The two-dimensional unit cell is shown in Fig. 2 with $\vec{a}_1=a\hat{x}$ and $\vec{a}_2=a\hat{y}$ where $a=\sqrt{2}r_0$ and $\hat{x}$ and $\hat{y}$ are unit vectors in the x and y directions. In all planes for which l_3 is zero or an even integer, the lattice site on the z axis is occupied by a positive ion; in those planes for which l_3 is an odd integer, this site is occupied by a negative ion. We therefore adopt the following conventions concerning the label j and the vectors $\vec{s}_j$. The value $j=1$ will denote a positive ion, and $j=2$ will denote a negative ion. However, the vectors $\vec{s}_j$ must be chosen as $\vec{s}_1=0$, $\vec{s}_2=\frac{1}{2}a(\hat{x}+\hat{y})$ for planes with l_3 zero or an even integer, and as $\vec{s}_1=\frac{1}{2}a(\hat{x}+\hat{y})$, $\vec{s}_2=0$ for planes with l_3 an odd integer in order to maintain a common origin for the lattice vectors $\vec{l}$ in all planes.

When the ions are displaced from their equilibrium positions we define $u_{\alpha j}(\vec{l}, l_3)$ to be the αth Cartesian component of the displacement of the ion of type j in the unit cell located by the two-dimensional vector $\vec{l}$ in the plane labeled by l_3. The vector locating ion j in unit cell l of plane l_3 is then

$$\vec{r}(\vec{l}, l_3, j)=l_3r_0\hat{z}+\vec{l}+\vec{s}_j+\vec{u}_j(\vec{l}, l_3)\,,$$

and in equilibrium

$$\vec{r}(\vec{l}, l_3, j)=\vec{r}^{\,0}(\vec{l}, l_3, j)=l_3r_0\hat{z}+\vec{l}+\vec{s}_j\,.$$

We now write the equations of motion of the lattice simply as

$$m_j\ddot{u}_{\alpha j}(\vec{l}, l_3)=F^S_{\alpha j}(\vec{l}, l_3)+F^C_{\alpha j}(\vec{l}, l_3)\,. \qquad (2.1)$$

The right-hand side of these equations represents the αth component of the total force acting on the ion labeled by j, $\vec{l}$, and l_3 when the ions are displaced from their equilibrium positions. The first term $F^S_{\alpha j}(\vec{l}, l_3)$ represents that part of the total force arising from the short-range interactions be-

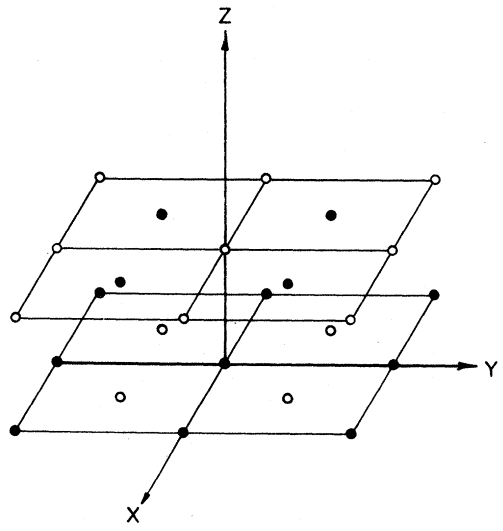

FIG. 1. Coordinate system used in calculation of normal modes. Solid circles represent positive ions. Empty circles represent negative ions.

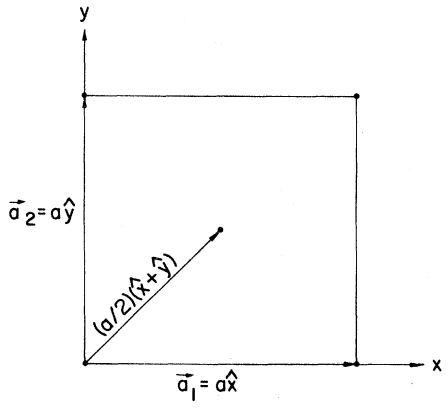

FIG. 2. Two-dimensional unit cell of the plane lattice.

tween neighboring ions and $F^C_{\alpha j}(\vec{l}, l_3)$ represents the electromagnetic forces.

In the harmonic approximation we assume that these forces can be written in the form

$$F^{(S,C)}_{\alpha j}(\vec{l}, l_3) = -\sum_{\substack{\beta, j', \\ \vec{l}', l_3'}} \Phi^{(S,C)}_{\alpha\beta}(\vec{l}, \vec{l}'; l_3, l_3'; j, j') \times u_{\beta j'}(\vec{l}', l_3') . \quad (2.2)$$

We next write the displacements in the form

$$u_{\alpha j}(\vec{l}, l_3) = \frac{w_{\alpha j}(l_3)}{\sqrt{m_j}} e^{i\vec{q}\cdot\vec{l}} e^{-i\omega t} , \quad (2.3)$$

where $\vec{q}$ is the two-dimensional wave vector in the plane of the slab and is such that the displacements satisfy periodic boundary conditions in the x and y directions.

Using Eqs. (2.2) and (2.3) the equations of motion of the lattice may then be written as

$$-\omega^2 w_{\alpha j}(l_3) + \sum_{\beta, j', l_3'} [D^S_{\alpha\beta}(\vec{q}; l_3, l_3'; j, j') + D^C_{\alpha\beta}(\vec{q}; l_3, l_3'; j, j')] w_{\beta j'}(l_3') = 0 , \quad (2,4)$$

where

$$D^{(S,C)}_{\alpha\beta}(\vec{q}; l_3, l_3'; j, j') = (m_j m_j')^{-1/2} \times \sum_{\vec{l}'} \Phi^{(S,C)}_{\alpha\beta}(\vec{l}, \vec{l}'; l_3, l_3'; j, j') e^{i\vec{q}\cdot(\vec{l}'-\vec{l})} . \quad (2.5)$$

Equation (2.4) leads to a $6N \times 6N$ matrix whose eigenvalues ω_m^2, $m = 1, 2, \ldots, 6N$, are the squares of the normal-mode frequencies of the slab. The eigenvectors give the pattern of ionic displacement amplitudes across the slab.

III. MATRIX $D^S_{\alpha\beta}(\vec{q}; l_3, l_3'; j, j')$

In this section we consider those short-range repulsive forces arising from the overlap of the electron clouds of neighboring ions. Following Kellermann,[9] we treat these forces as being derivable from a central potential $\Phi(r)$ and include interactions between nearest neighbors only.

We define two constants A and B by

$$A = \frac{4r_0^3}{e^2} \frac{d^2\Phi}{dr^2}\bigg|_{r=r_0} , \quad (3.1)$$

$$B = \frac{4r_0^2}{e^2} \frac{d\Phi}{dr}\bigg|_{r=r_0} . \quad (3.2)$$

All of the nonzero elements of $D^S_{\alpha\beta}$ are listed below:

For $l_3 \neq l_3'$, $j \neq j'$:

$$D^S_{xx}(\vec{q}; l_3, l_3'; j, j') = D^S_{yy}(\vec{q}; l_3, l_3'; j, j') = -\frac{e^2}{4r_0^3(m_j m_{j'})^{1/2}} B(\delta_{l_3, l_3'+1} + \delta_{l_3, l_3'-1}) , \quad (3.3)$$

$$D^S_{zz}(\vec{q}; l_3, l_3'; j, j') = -\frac{e^2}{4r_0^3(m_j m_{j'})^{1/2}} A \times (\delta_{l_3, l_3'+1} + \delta_{l_3, l_3'-1}) . \quad (3.4)$$

For $l_3 = l_3'$, $j \neq j'$:

$$D^S_{xx}(\vec{q}; l_3, l_3; j, j') = D^S_{yy}(\vec{q}; l_3, l_3; j, j') = -\frac{e^2}{2r_0^3(m_j m_{j'})^{1/2}} (A+B) e^{i\vec{q}\cdot(\vec{s}_j - \vec{s}_{j'})} \times \cos\tfrac{1}{2}q_x a \cos\tfrac{1}{2}q_y a , \quad (3.5)$$

$$D^S_{zz}(\vec{q}; l_3, l_3; j, j') = -\frac{e^2}{r_0^3(m_j m_{j'})^{1/2}} B e^{i\vec{q}\cdot(\vec{s}_j - \vec{s}_{j'})} \times \cos\tfrac{1}{2}q_x a \cos\tfrac{1}{2}q_y a , \quad (3.6)$$

$$D^S_{xy}(\vec{q}; l_3, l_3; j, j') = D^S_{yx}(\vec{q}; l_3, l_3; j, j') = \frac{e^2}{2r_0^3(m_j m_{j'})^{1/2}} (A-B) e^{i\vec{q}\cdot(\vec{s}_j - \vec{s}_{j'})} \times \sin\tfrac{1}{2}q_x a \sin\tfrac{1}{2}q_y a . \quad (3.7)$$

For $l_3 = l_3'$, $j = j'$, and l_3 not a surface layer:

$$D^S_{\alpha\beta}(\vec{q}; l_3, l_3; j, j) = \delta_{\alpha\beta}(e^2/r_0^3 m_j)(\tfrac{1}{2}A + B) . \quad (3.8)$$

For $l_3 = l_3'$, $j = j'$, and l_3 a surface layer:

$$D^S_{xx}(\vec{q}; l_3, l_3; j, j) = D^S_{yy}(\vec{q}; l_3, l_3; j, j) = (e^2/r_0^3 m_j)(\tfrac{1}{2}A + \tfrac{3}{4}B) , \quad (3.9)$$

$$D^S_{zz}(\vec{q}; l_3, l_3; j, j) = (e^2/r_0^3 m_j)(\tfrac{1}{4}A + B) . \quad (3.10)$$

IV. MATRIX $D^C_{\alpha\beta}(\vec{q}; l_3, l_3'; j, j')$

We now turn our attention to the electromagnetic

forces which act on the ions in the slab. We will initially include the effects of retardation of the Coulomb forces and will find that the $D^C_{\alpha\beta}(\vec{q}; l_3, l_3'; j, j')$ depend upon the frequency of oscillation ω of the lattice, as well as the wave vector $\vec{q}$. Upon letting the speed of light c become infinite in these expressions, they become independent of ω and represent the unretarded Coulomb forces.

We first consider a point ion of charge e executing simple harmonic motion of frequency ω about an equilibrium position $\vec{r}=\vec{r}_0$ with amplitude $\vec{u}$. This ion will give rise to an electric field at the point $\vec{r}$ given by[10]

$$\vec{E}(\vec{r}, t)=e[(\omega^2/c^2)\vec{u}+(\vec{u}\cdot\vec{\nabla})\vec{\nabla}] \times \frac{\exp[i(\omega/c)|\vec{r}-\vec{r}_0|]}{|\vec{r}-\vec{r}_0|} e^{-i\omega t} . \quad (4.1)$$

In an ionic-crystal slab the electromagnetic force acting on an ion at a site fixed by $\vec{l}$, l_z, and $\vec{s}_j$ is simply the Lorentz force $\vec{f}=e_j(\vec{E}+\vec{v}\times\vec{B}/c)$, where $\vec{E}$ and $\vec{B}$ are the electric and magnetic fields at the location of the ion arising from the motion of all the other ions in the slab, and $\vec{v}$ is the velocity of the reference ion, The $\vec{v}\times\vec{B}$ term depends quadratically upon the ionic displacements so, in the harmonic approximation, we take

$$F^C_{\alpha j}(\vec{l}, l_3)=e_j E_\alpha(\vec{r}(\vec{l}, l_3, j))=e_j \sum_{\substack{\beta, j' \\ \vec{l}', l_3'}}{}' e_{j'} u_{\beta j}(\vec{l}', l_3') \times\left[\frac{\omega^2}{c^2}\delta_{\alpha\beta}+\frac{\partial^2}{\partial x_\alpha \partial x_\beta}\right] \frac{\exp[i(\omega/c)|\vec{r}-\vec{r}(\vec{l}', l_3', j')|]}{|\vec{r}-\vec{r}(\vec{l}', l_3', j')|}\Bigg|_{\vec{r}=\vec{r}(\vec{l}, l_3, j)} , \quad (4.2)$$

where the prime on the sum indicates the exclusion of the point $\vec{l}'=\vec{l}$, $l_3'=l_3$, $j'=j$. We choose $\vec{l}=0$; Eqs. (4.2), (2.2), (2.3), and (2.5) then lead directly to the expression

$$D^C_{\alpha\beta}(\vec{q}; l_3, l_3'; j, j')=-\frac{e_j e_{j'}}{(m_j m_{j'})^{1/2}} \times \lim_{\substack{\vec{r}\to\vec{s}_j-\vec{s}_{j'} \\ +(l_3-l_3')\hat{z}}}\left[\frac{\omega^2}{c^2}\delta_{\alpha\beta}+\frac{\partial^2}{\partial x_\alpha \partial x_\beta}\right]\sum_{\vec{l}'}{}' \frac{e^{i(\omega/c)|\vec{r}-\vec{l}'|}}{|\vec{r}-\vec{l}'|} e^{i\vec{q}\cdot\vec{l}'}, \quad (4.3)$$

where the prime on this sum indicates that, for $l_3'=l_3$, $j'=j$, we must exclude the point $\vec{l}'=0$ from the sum. Those elements of D^C for which $l_3'=l_3$ will require special considerations, as we shall later see.

The sums involved in Eq. (4.3) are slowly convergent and must be transformed to more rapidly convergent sums for practical numerical evaluation. For the case $l_3'\neq l_3$, we write

$$\sum_{\vec{l}} \frac{e^{i(\omega/c)|\vec{r}-\vec{l}|}}{|\vec{r}-\vec{l}|} e^{i\vec{q}\cdot\vec{l}}=\sum_{\vec{G}} A_G(z) e^{i(\vec{q}+\vec{G})\cdot\vec{x}} , \quad (4.4)$$

where

$$A_G(z)=\frac{1}{a_c}\int_{\text{cell}} \sum_{\vec{l}} \frac{e^{i(\omega/c)|\vec{r}-\vec{l}|}}{|\vec{r}-\vec{l}|} e^{i(\vec{q}+\vec{G})\cdot(\vec{l}-\vec{x})} d^2x . \quad (4.5)$$

The vectors $\vec{G}$ are the reciprocal-lattice vectors of the two-dimensional lattice in the plane of the slab and are defined by $\vec{G}=n_1\vec{b}_1+n_2\vec{b}_2$ where n_1 and n_2 are integers and $\vec{b}_1=(2\pi/a)\hat{x}$, $\vec{b}_2=(2\pi/a)\hat{y}$. Also, $\vec{x}$ is the projection of $\vec{r}$ on the xy plane, a_c is the area of a unit cell of the plane lattice, and $\int_{\text{cell}}$ denotes integration over the area of a unit cell.

By converting the expression for $A_G(z)$ into an integral over the entire xy plane, we find

$$A_G(z)=\frac{2\pi}{a_c}\int_0^\infty \frac{e^{i(\omega/c)(z^2+\rho^2)^{1/2}}}{(z^2+\rho^2)^{1/2}} J_0(|\vec{q}+\vec{G}|\rho)\rho\, d\rho , \quad (4.6)$$

where J_0 is the Bessel function of order zero. This integral depends upon the relative magnitudes of $|\vec{q}+\vec{G}|$ and ω/c.[11] For $|\vec{q}+\vec{G}|>\omega/c$:

$$A_G(z)=2\pi e^{-\alpha_G|z|}/(a_c\alpha_G) , \quad (4.7a)$$

where

$$\alpha_G=[(\vec{q}+\vec{G})^2-\omega^2/c^2]^{1/2} .$$

For $|\vec{q}+\vec{G}|<\omega/c$:

$$A_G(z)=i\,2\pi e^{i\beta_G|z|}/(a_c\beta_G), \quad (4.7b)$$

where

$$\beta_G=[\omega^2/c^2-|\vec{q}+\vec{G}|^2]^{1/2} .$$

For values of $\vec{q}$ in the first Brillouin zone, we note that if $q>\omega/c$ then all $A_G(z)$ will be given by Eq. (4.7a). However, if $q<\omega/c$ then $A_{G=0}(z)$ will be given by Eq. (4.7b) and all other $A_G(z)$ will be given by Eq. (4.7a). Thus, if $q>\omega/c$ and $l_3'\neq l_3$, Eqs. (4.3), (4.4), (4.6), and (4.7a) give

$$D^C_{\alpha\beta}(\vec{q}; l_3, l_3'; j, j')=-\frac{2\pi e_j e_{j'}}{a_c(m_j m_{j'})^{1/2}}\sum_{\vec{G}} \lim_{\vec{r}\to\vec{s}_j-\vec{s}_{j'}+(l_3-l_3')\hat{z}}\left[\frac{\omega^2}{c^2}\delta_{\alpha\beta}+\frac{\partial^2}{\partial x_\alpha\partial x_\beta}\right]\frac{e^{-\alpha_G|z|}}{\alpha_G} e^{i(\vec{q}+\vec{G})\cdot\vec{x}} . \quad (4.8)$$

The explicit expressions for these elements are given below.

For $\alpha, \beta = x, y$:

$$D^C_{\alpha\beta}(\vec{q};\, l_3, l_3';\, j,\, j') = -\frac{2\pi e_j e_{j'}}{a_c(m_j m_{j'})^{1/2}} \sum_{\vec{G}} [(\omega^2/c^2)\delta_{\alpha\beta} - (q+G)_\alpha (q+G)_\beta] \frac{e^{-\alpha_G |l_3 - l_3'| r_0}}{\alpha_G} e^{i(\vec{q}+\vec{G})\cdot(\vec{s}_j - \vec{s}_{j'})} . \quad (4.9)$$

For $\alpha = x, y$:

$$D^C_{\alpha z}(\vec{q};\, l_3, l_3';\, j,\, j') = D^C_{z\alpha}(\vec{q};\, l_3, l_3';\, j,\, j')$$
$$= i \frac{2\pi e_j e_{j'}}{a_c(m_j m_{j'})^{1/2}} \frac{(l_3 - l_3')}{|l_3 - l_3'|} \sum_{\vec{G}} (q+G)_\alpha e^{-\alpha_G |l_3 - l_3'| r_0} e^{i(\vec{q}+\vec{G})\cdot(\vec{s}_j - \vec{s}_{j'})} . \quad (4.10)$$

For $\alpha = \beta = z$:

$$D^C_{zz}(\vec{q};\, l_3, l_3';\, j,\, j') = -\frac{2\pi e_j e_{j'}}{a_c(m_j m_{j'})^{1/2}} \sum_{\vec{G}} |\vec{q}+\vec{G}|^2 \times \frac{e^{-\alpha_G |l_3 - l_3'| r_0}}{\alpha_G} e^{i(\vec{q}+\vec{G})\cdot(\vec{s}_j - \vec{s}_{j'})} . \quad (4.11)$$

To obtain the corresponding expressions for $q < \omega/c$, one simply replaces $(q^2 - \omega^2/c^2)^{1/2}$ by $-i(\omega^2/c^2 - q^2)^{1/2}$ in the $\vec{G} = 0$ term of each of the above sums.

We now turn our attention to the case $l_3' = l_3$ and first consider $j' \neq j$. The preceding expressions, valid for $l_3' \neq l_3$, contain sums which diverge for $l_3' = l_3$. In this case we modify our treatment by using one-dimensional rather than two-dimensional Fourier transformations. We write

$$\sum_{\vec{l}} \frac{e^{i(\omega/c)|\vec{x} - \vec{l}|}}{|\vec{x} - \vec{l}|} e^{i\vec{q}\cdot\vec{l}} = \sum_{l_y} \sum_{G_x} B_{G_x}(y - l_y) e^{i(q_x + G_x)x} e^{iq_y l_y} , \quad (4.12)$$

where

$$B_{G_x}(y - l_y) = \frac{1}{a} \int_{-\infty}^{\infty} \frac{e^{i(\omega/c)[x^2 + (y - l_y)^2]^{1/2}}}{[x^2 + (y - l_y)^2]^{1/2}} e^{-i(q_x + G_x)x} dx . \quad (4.13)$$

q_x and q_y are the x and y components of $\vec{q}$, and l_x and l_y are the x and y components of $\vec{l}$, respectively. This integral depends upon the relative magnitudes of $|q_x + G_x|$ and ω/c.[11]

For $|q_x + G_x| > \omega/c$:

$$B_{G_x}(y - l_y) = (2/a) K_0([(q_x + G_x)^2 - \omega^2/c^2]^{1/2} |y - l_y|) . \quad (4.14a)$$

For $|q_x + G_x| < \omega/c$:

$$B_{G_x}(y - l_y) = i(\pi/a) H_0^{(1)}([\omega^2/c^2 - (q_x + G_x)^2]^{1/2} |y - l_y|) . \quad (4.14b)$$

Here K_0 is the modified Bessel function of order zero, and $H_0^{(1)}$ is the Hankel function of the first kind of order zero.

Considering the case $|q_x| > \omega/c$ we combine Eqs. (4.12) and (4.14a) to obtain

$$\sum_{\vec{l}} \frac{e^{i(\omega/c)|\vec{x} - \vec{l}|}}{|\vec{x} - \vec{l}|} e^{i\vec{q}\cdot\vec{l}} = (2/a) \sum_{l_y} \sum_{G_x} K_0([(q_x + G_x)^2 - \omega^2/c^2]^{1/2} |y - l_y|) e^{i(q_x + G_x)x} e^{iq_y l_y} . \quad (4.15)$$

Using Eqs. (4.3) and (4.15) we may obtain, for example,

$$D^C_{xx}(\vec{q};\, l_3, l_3';\, j,\, j') = -\frac{2e_j e_{j'}}{a(m_j m_{j'})^{1/2}} \sum_{l_y} \sum_{G_x} [\omega^2/c^2 - (q_x + G_x)^2] e^{i(q_x + G_x)(s_{jx} - s_{j'x})} \times K_0([(q_x + G_x)^2 - \omega^2/c^2]^{1/2} |l_y + s_{j'y} - s_{jy}|) e^{iq_y l_y} . \quad (4.16)$$

In treating the case $l_3' = l_3$ and $j' = j$, we again use the transformation defined by Eqs. (4.12) through (4.15) for $|q_x| > \omega/c$ to obtain, for example,

$$D^C_{xx}(\vec{q};\, l_3, l_3';\, j,\, j) = \frac{1}{m_j} \Phi^C_{xx}(0, 0;\, l_3, l_3;\, j,\, j) - \frac{2e_j^2}{am_j} \sum_{l_y}{}' \sum_{G_x} [\omega^2/c^2 - (q_x + G_x)^2] \times K_0([(q_x + G_x)^2 - \omega^2/c^2]^{1/2} |l_y|) e^{iq_y l_y} - B_x(\vec{q}, j) . \quad (4.17)$$

Here $\Phi^C_{xx}(0, 0;\, l_3, l_3;\, j,\, j)$ represents the force which acts on the reference ion of type j at $\vec{l} = 0$ in layer l_3 if it is displaced from equilibrium while all other ions remain fixed. The prime on the sum over l_y here denotes the exclusion of those terms for which $l_y = 0$. The term $-B_x(\vec{q}, j)$ is then the contribution to $D^C_{xx}(\vec{q};\, l_3, l_3;\, j,\, j)$ from all ions in the line $l_y = 0$ except the reference ion at $l_x = 0$.

Excluding retardation, $\Phi^C_{xx}(0, 0;\, l_3, l_3;\, j, j)$ would be given by

$$\Phi^{CU}_{xx}(0, 0;\, l_3, l_3;\, j, j) = -\sum_{\vec{l}, l_3', j'}{}' \Phi^{CU}_{xx}(0, \vec{l}\,', l_3, l_3';\, j, j') . \quad (4.18)$$

The superscript U indicates that these are matrix

elements of the unretarded Coulomb interactions. In order to include retardation we must use the fact that the reference ion of charge e_j not only experiences this force due to the electrostatic field of all the other fixed ions but also radiates power due to its acceleration as it oscillates about its equilibrium position. This is taken into account by introducing a frequency-dependent effective force acting on the reference ion given by[10]

$$\vec{f} = \frac{2}{3}\frac{e_j^2}{c^3}\frac{d^3\vec{u}_j(0, l_3)}{dt^3} ,$$

which leads us to

$$\Phi^C_{\alpha\alpha}(0, 0; l_3, l_3; j, j) = \Phi^{CU}_{\alpha\alpha}(0, 0; l_3, l_3; j, j) - \tfrac{2}{3} i e_j^2 \omega^3/c^3 , \quad (4.19)$$

for $\alpha = x$, y, and z.

An expression for $B_x(\vec{q}, j)$ is found by expanding Eq. (4.3) for $l_3' = l_3$ and $l_y = 0$. This yields

$$B_x(\vec{q}, j) = \frac{2e_j^2}{m_j}\sum_{l_x}{}' \frac{e^{i(\omega/c)|l_x|}}{l_x} \times \left(\frac{1}{|l_x|^2} - i\frac{\omega}{c}\frac{1}{|l_x|}\right) e^{iq_x l_x} , \quad (4.20)$$

where the primed sum excludes $l_x = 0$.

Expressions for various elements of D^C with $l_3' = l_3$ are given in Appendix A assuming $|q_\gamma| > \omega/c$ where γ is either x or y depending upon the particular element of D^C. One can easily obtain the corresponding expressions for these matrix elements if the inequality is reversed ($|q_\gamma| < \omega/c$) by using Eq. (4.14b).

It can be shown that the matrix D^C is Hermitian only for $q > \omega/c$. Thus the eigenvalues of the matrix $D^S + D^C$ will necessarily be real only for the nonradiative region $q > \omega/c$. (The matrix D^S is obviously Hermitian for all $\vec{q}$.)

The elements of D^C excluding retardation are listed in Appendix B.

V. GENERAL THEORY OF INFRARED OPTICAL PROPERTIES

We now consider the response of an ionic-crystal slab to an externally applied electromagnetic field. In particular, we will develop a theory from which the transmittance, reflectance, and absorptance of the slab may be computed as a function of the frequency of the applied field at any angle of incidence.

With an externally applied force, the equations of motion of the lattice are obtained by adding the applied force to the right-hand side of Eq. (2.1). This gives

$$m_j \ddot{u}_{\alpha j}(\vec{l}, l_3) = F^S_{\alpha j}(\vec{l}, l_3) + F^C_{\alpha j}(\vec{l}, l_3) + F^e_{\alpha j}(\vec{l}, l_3) , \quad (5.1)$$

where $F^e_{\alpha j}(\vec{l}, l_3)$ is the αth component of the applied force acting on the ion labeled by the j, $\vec{l}$, and l_3. Development of a theory of the optical properties of the slab requires further consideration of the term $F^C_{\alpha j}(\vec{l}, l_3)$ which arises from the electromagnetic field within the slab. We separate this field into two parts—the long-wavelength macroscopic field which occurs in Maxwell's equations and the local field, which is a sum of all short-wavelength components. The total macroscopic field can then be obtained as a superposition of this induced macroscopic field and the applied field. This treatment will give expressions for the total field both within the slab and in regions away from the slab. The optical properties will then follow easily.

We first examine the components of $D^C_{\alpha\beta}(\vec{q}; l_3, l_3'; j, j')$ as given in Sec. IV, keeping in mind that in treating the infrared optical properties of the slab we will have $q \leq \omega/c \simeq 10^3$ cm^{-1}, while the smallest nonzero reciprocal-lattice vectors have a magnitude of $2\pi/a \simeq 10^8$ cm^{-1}.

In this long-wavelength region all elements of the matrix D^C can be written in the form

$$D^C_{\alpha\beta}(\vec{q}; l_3, l_3'; j, j') = D^M_{\alpha\beta}(\vec{q}; l_3, l_3'; j, j') + D^L_{\alpha\beta}(l_3, l_3'; j, j') , \quad (5.2)$$

where the superscripts M and L denote those parts of D^C arising from the macroscopic and local fields, respectively. For $l_3' \neq l_3$, the D^M are simply the $\vec{G} = 0$ terms of the sums appearing in the expressions for D^C and the remaining $\vec{G} \neq 0$ terms make up D^L.[12] Because of the special treatment required in the case $l_3' = l_3$, the above separation of D^C is not as straightforward as in the case $l_3' \neq l_3$. The result of this separation is that the approximate expressions for D^M are the same as the corresponding elements for $l_3' \neq l_3$ with $l_3 - l_3'$ taken to be zero.

The induced macroscopic and local electric field at an ion of type j in layer l_3 are given by

$$E^{(M,L)}_\alpha(l_3, j) = -(\sqrt{m_j}/e_j) \times \sum_{\beta, j', l_3'} D^{(M,L)}_{\alpha\beta}(\vec{q}; l_3, l_3'; j, j') w_{\beta j'}(l_3) . \quad (5.3)$$

In the limit of a uniformly polarized infinite crystal, evaluation of the local field yields $E^L_\alpha(l_3, j) = \frac{4}{3}\pi P_\alpha$, where $\vec{P}$ is the polarization of the crystal. This is the usual Lorentz local field and is independent of the ion type j.

In order to determine the optical properties of the slab, we assume the external force to be due to an electromagnetic plane wave incident on the slab from the negative-z side. If we let $\vec{K}$ be the wave vector of this wave, then its projection parallel to the slab is given by $\vec{k} = (\omega/c)\sin\theta\hat{k}$, where $\hat{k}$ is a unit vector in the plane of the slab and θ is the angle

of incidence; its z component is $K_z=(\omega/c)\cos\theta$. We therefore write

$$F^e_{\alpha j}(\vec{l}, l_3)=e_j E^e_\alpha(l_3)e^{i\vec{k}\cdot(\vec{l}+\vec{s}_j)} \tag{5.4}$$

and

$$E^e_\alpha(l_3)=E^e_\alpha e^{iK_z l_3 r_0}\,. \tag{5.5}$$

If we make a normal coordinate expansion of the ionic displacements in terms of the eigenvectors of the matrix $D^S_{\alpha\beta}(\vec{q};\ l_3,\ l_3';\ j,\ j')+D^L_{\alpha\beta}(l_3,\ l_3';\ j, j')$, we may then solve the equation of motion (5.1) for the displacements as

$$w_{\alpha j}(l_3)=\sum_{\substack{\beta, j', \\ l_3', m}} \frac{e_{j'}}{\sqrt{m_{j'}}}\,\frac{\epsilon^{m*}_{\beta j'}(\vec{k}, l_3')\epsilon^m_{\alpha j}(\vec{k}, l_3)}{\omega_m^2-\omega^2} \times[E^M_\beta(l_3')+E^e_\beta(l_3')]\,, \tag{5.6}$$

where we have dropped the index j in $\vec{E}^M$ since it is independent of j in the long-wavelength region. The index m labels the normal modes of the matrix D^S+D^L; the ϵ^m are its eigenvectors and the ω_m^2 are its eigenvalues.

Equation (5.6) relates the ionic displacements to the total macroscopic field, $\vec{E}^T=\vec{E}^M+\vec{E}^e$, within the crystal. Inserting this equation into Eq. (5.3) yields

$$E^M_\alpha(l_3)=\sum_{\beta, l_3'} M_{\alpha\beta}(l_3,\ l_3')E^T_\beta(l_3')\,, \tag{5.7}$$

where

$$M_{\alpha\beta}(l_3,\ l_3')=-\sum_{\substack{j, j', \gamma, \\ l_3'', m}} D^M_{\alpha\gamma}(\vec{k};\ l_3,\ l_3'',\ j,\ j') \times\frac{\epsilon^{m*}_{\beta j}(\vec{k}, l_3')\epsilon^m_{\gamma j'}(\vec{k}, l_3'')}{\omega_m^2-\omega^2}\,. \tag{5.8}$$

If we now add $E^e_\alpha(l_3)$ to both sides of Eq. (5.7), we obtain

$$\sum_{\beta, l_3'}[\delta_{\alpha\beta}\delta_{l_3 l_3'}-M_{\alpha\beta}(l_3,\ l_3')]E^T_\beta(l_3')=E^e_\alpha(l_3)\,. \tag{5.9}$$

For a slab of N layers of ions, this is a set of $3N$ linear inhomogeneous equations which may be solved numerically for the amplitude of the total macroscopic field at each layer of the slab in terms of the applied field. Having solved for the total macroscopic field within the slab, we can now calculate the field in regions away from the slab directly from Eq. (5.7). We simply replace $l_3 r_0$ by z to obtain

$$E^M_\alpha(z)=\sum_{\beta, l_3'} M_{\alpha\beta}(z, l_3')E^T_\beta(l_3')\,, \tag{5.10}$$

which holds for all values of z.

To examine this more closely we write out Eq. (5.10) explicitly as

$$E^M_\alpha(z)=-\sum_{\beta, l_3'}\frac{2\pi i}{a_c}\sum_{\substack{j, j', \gamma, \\ l_3'', m}}\frac{e_j e_{j'}}{(m_j m_{j'})^{1/2}}\left[\frac{\omega^2}{c^2}\delta_{\alpha\gamma}-K_\alpha(z-l_z'')K_\gamma(z-l_z'')\right] \times\frac{\epsilon^{m*}_{\beta j}(\vec{k}, l_3')\epsilon^m_{\gamma j'}(\vec{k}, l_3'')}{\omega_m^2-\omega^2}\exp[i(\omega^2/c^2-|\vec{k}|^2)^{1/2}|z-l_3'' r_0|]E^T_\beta(l_3')\,, \tag{5.11}$$

where

$$\vec{K}(z-l_z)=\left[k_x,\ k_y,\ \frac{z-l_z}{|z-l_z|}\left(\frac{\omega^2}{c^2}-|\vec{k}|^2\right)^{1/2}\right]. \tag{5.12}$$

Since $|\vec{k}|^2=(\omega^2/c^2)\sin^2\theta$, we have

$$(\omega^2/c^2-|\vec{k}|^2)^{1/2}=(\omega/c)\cos\theta=K_z\,. \tag{5.13}$$

which is the component of the wave vector of the applied field normal to the slab. Thus, by inspection of Eq. (5.11), the induced macroscopic field within the slab is a sum of fields traveling in both the positive- and negative-z directions, while in regions removed from the slab, it is a field traveling away from the slab with wave vector $\vec{K}=(\omega/c)\hat{K}$.

Intrinsic damping in the crystal may be put into this theory in a phenomenological way by introducing a damping force $-m_j\gamma\dot{u}_{\alpha j}(\vec{l}, l_3)$ on the right-hand side of the equation of motion of the lattice (3.1), where γ is the damping constant of the lattice. By tracing this term through the steps leading to Eq. (5.9), it is easily seen that this is equivalent to replacing the denominator $\omega_m^2-\omega^2$ in Eq. (5.8) by $\omega_m^2-\omega^2-i\gamma\omega$.

In order to calculate the transmittance, reflectance, and absorptance of the slab we assume the applied field to be traveling in the positive-z direction throughout all space and simply use the principle of superposition to calculate the transmitted and reflected fields. The transmitted field is then

$$E^T_\alpha(z+)=E^M_\alpha(z+)+E^e_\alpha(z+) \tag{5.14}$$

and the reflected field is simply

$$E^R_\alpha(z-)=E^M_\alpha(z-)\,,$$

where $z+$ and $z-$ denote the regions of space away from the slab in the positive- and negative-z directions, respectively.

The optical properties of the slab follow directly from the above expressions for the transmitted and

reflected fields. Expressions for the transmittance, reflectance, and absorptance for the cases of P and S polarizations of the incident field will be derived in the Secs. VI and VII.

VI. P POLARIZATION

In the case of P polarization the incident electric field vector is polarized in the plane of incidence. We choose the xz plane as the plane of incidence so that $K_x = (\omega/c)\sin\theta$, $K_y = 0$, and $K_z = (\omega/c)\cos\theta$ where θ is the angle of incidence measured from the normal to the slab.

We first solve Eq. (5.9) for the amplitude of the total macroscopic field at each layer of the slab. We further approximate the eigenvectors $\epsilon^m_{\alpha j}(\vec{k}, l_3)$ appearing in the expression for $M_{\alpha\beta}(l_3, l_3')$ by their $\vec{k}=0$ values since we are working in the infrared region.[13] We then have no coupling of the y components of the ionic displacements and fields with their x and z components because the $\vec{k}=0$ eigenvectors are such that

$$M_{xy}(l_3, l_3') = M_{yx}(l_3, l_3') = M_{zy}(l_3, l_3') = M_{yz}(l_3, l_3') = 0 \ . \tag{6.1}$$

Equation (5.9) thus separates into a set of $2N$ linear inhomogeneous equations for $\alpha = x, z$ and a set of N linear homogeneous equations for $\alpha = y$ since $E_y = 0$. The N homogeneous equations simply give the y-polarized normal modes of the slab, which have no effect on the P polarization optical properties. The remaining $2N$ inhomogeneous equations may then be solved numerically for $E^T_x(l_3)$ and $E^T_z(l_3)$ which then permit calculation of the transmitted and reflected fields from Eqs. (5.10), (5.14), and (5.15).

We choose the applied electric field to be of unit magnitude such that

$$E^e_x = -\cos\theta\, e^{i(\vec{K}\cdot\vec{r}-\omega t)} \ , \qquad E^e_y = 0 \ , \qquad E^e_z = \sin\theta\, e^{i(\vec{K}\cdot\vec{r}-\omega t)} \ . \tag{6.2}$$

By inspection of Eq. (5.10) with the $M_{\alpha\beta}(z, l_3')$ written out explicitly we can see that the total field on the transmission side of the slab is such that

$$E^T_z(z+) = -\tan\theta\, E^T_x(z+) \ , \tag{6.3}$$

and the reflected field is such that

$$E^R_z(z-) = \tan\theta\, E^R_x(z-) \ . \tag{6.4}$$

Thus one needs only to calculate $E^T_x(z+)$ and $E^R_x(z-)$ directly from Eq. (5.10).

The transmittance of the slab is defined as

$$T = |\vec{S}^T| / |\vec{S}^e| \ , \tag{6.5}$$

where $\vec{S}^T$ and $\vec{S}^e$ are the time-averaged Poynting vectors of the transmitted and incident fields, respectively, and are given by

$$\vec{S}^T = (c/8\pi)\,\mathrm{Re}[\,\vec{E}^{T*}(z+)\times\vec{H}^T(z+)\,] \ ,$$
$$\vec{S}^e = (c/8\pi)\,\mathrm{Re}(\,\vec{E}^{e*}\times\vec{H}^e\,) \ . \tag{6.6}$$

Here $\vec{H}$ is the magnetic field and is determined from the Maxwell equation

$$i\vec{K}\times\vec{E} = i(\omega/c)\,\vec{H} \ . \tag{6.7}$$

Calculation of $\vec{S}^T$ and $\vec{S}^e$ from Eq. (6.6) gives

$$T = E^{T*}_x(z+)E^T_x(z+)/\cos^2\theta \ . \tag{6.8}$$

The reflectance of the slab is calculated in a similar fashion and is found to be

$$R = E^{R*}_x(z-)E^R_x(z-)/\cos^2\theta \ . \tag{6.9}$$

The absorptance is then calculated from

$$A = 1 - T - R \ . \tag{6.10}$$

VII. S POLARIZATION

In the case of S polarization the incident electric field vector is polarized normal to the plane of incidence. We again choose an angle of incidence θ in the xz plane as in the case of P polarization. Here we have

$$E^e_x = 0 \ , \quad E^e_y = e^{i(\vec{K}\cdot\vec{r}-\omega t)} \ , \quad E^e_z = 0 \ . \tag{7.1}$$

We again approximate the normal-mode eigenvectors appearing in the $M_{\alpha\beta}(l_3, l_3')$ by their $\vec{k}=0$ values so that in Eq. (5.9) the y motion separates from the xz motion as a set of N linear inhomogeneous equations which may be solved for $E^T_y(l_3)$. We then calculate the transmitted and reflected fields from Eqs. (5.10), (5.14), and (5.15) as before.

The transmittance, reflectance, and absorptance in this case are easily found to be given by

$$T = E^{T*}_y(z+)E^T_y(z+) \ , \tag{7.2}$$

$$R = E^{R*}_y(z-)E^R_y(z-) \ , \tag{7.3}$$

$$A = 1 - T - R \ . \tag{7.4}$$

VIII. LOCAL APPROXIMATION

The preceding treatment of the infrared optical properties of the slab is local in the plane of the slab in the sense that the fields and ionic displacements are assumed to be essentially uniform over any given layer of ions in the slab. This assumption was used in replacing the eigenvectors $\epsilon^m_{\alpha j}(\vec{k}, l_3)$ by their $\vec{k}=0$ values and in replacing all $e^{i\vec{k}\cdot\vec{s}_j}$ factors by unity. However, the treatment is nonlocal in the direction normal to the slab in that no assumptions were made concerning the variation of the fields and ionic displacements from one layer of ions to the next. This is evident from the sums over layers, l_3, maintained throughout the theory.

This type of treatment seems reasonable in view of the fact that the externally applied field has a long wavelength and the component parallel to the

slab of the wave vector of the macroscopic field induced within the slab must be the same as that of the applied field. Any rapid variations in the total field within the slab must then take place in the direction normal to the slab; i.e., if we think of the dispersion relation for light in an infinite medium, $|\vec{K}|^2=\epsilon(\omega)\omega^2/c^2$, as applying to the slab, then any change in $|\vec{K}|$ resulting from a change in $\epsilon(\omega)$ near a resonance must show up as a change in the component of $\vec{K}$ normal to the slab since the parallel component of $\vec{K}$ is fixed at some small value by continuity across the surface of the slab.

We can modify our preceding treatment to obtain an approximation which is local in the direction normal to the slab as well as in the plane of the slab by assuming that the fields and ionic displacements are essentially uniform across the slab. The procedure for calculating the macroscopic fields and thus the optical properties is found to be the same as in the nonlocal case except that we replace $M_{\alpha\beta}(l_3, l_3')$, as given by Eq. (5.8), by

$$M_{\alpha\beta}^{\mathrm{LOC}}(l_3, l_3') = \frac{2\pi i r_0}{(\omega^2/c^2-|\vec{k}|^2)^{1/2}} \times \sum_{\gamma}[(\omega^2/c^2)\delta_{\alpha\beta}-K_\alpha(l_3-l_3')K_\gamma(l_3-l_3')] \times e^{i(\omega^2/c^2-|\vec{k}|^2)^{1/2}|l_3-l_3'|r_0}\chi_{\alpha\beta}(\omega)\,, \qquad (8.1)$$

where

$$\chi_{\alpha\beta}(\omega)=\frac{1}{Na_c r_0}\sum_{\substack{j,j',l_3,\\ l_3',m}}\frac{e_j e_{j'}}{(m_j m_{j'})^{1/2}} \times \frac{\epsilon_{\beta j}^{m}(0, l_3')\epsilon_{\gamma j}^{m}(0, l_3)}{\omega_m^2-\omega^2} \qquad (8.2)$$

is the local electric susceptibility of the slab.

The structure of $M_{\alpha\beta}^{\mathrm{LOC}}(l_3, l_3')$ is such that the computation of the optical properties in the local case is much simpler and less time consuming than in the nonlocal case.

We should emphasize that neither the procedure used in this local approximation nor that of the preceding nonlocal theory is the same as that used in classical electricity and magnetism. The major difference is that we assume the applied field to exist throughout all space and calculate the transmitted, reflected and incident fields by appropriate superpositions of the applied and induced fields in the regions of space on either side of the slab while, in a classical calculation, one normally assumes the existence of different fields in the three regions of space determined by the region occupied by the slab, the reflection side of the slab and the transmission side of the slab and then calculates the amplitudes of these fields from appropriate boundary conditions at the surfaces of the slab.

IX. NORMAL MODES OF VIBRATION

The unretarded normal modes of vibration of a NaCl crystal slab of seven layers of ions have been computed from the eigenvalue equation (2.4) using the dynamical matrix elements presented in Appendix B. The values of the physical constants used in the calculation are the same as those given by Tong and Maradudin.[3] They are

$$m_+(\mathrm{Na})=38.16\times10^{-24}\ \mathrm{g}, \qquad m_-(\mathrm{Cl})=58.85\times10^{-24}\ \mathrm{g},$$

$$r_0=2.814\times10^{-8}\ \mathrm{cm}, \qquad e=4.8\times10^{-10}\ \mathrm{esu},$$

$$A=9.288, \qquad B=-1.165.$$

The normal-mode eigenfrequencies and eigenvectors were calculated for $q_y=0$ with q_x ranging over various values from $q_x=0$ to the first zone boundary where $q_x=\pi/a$.

For $q_y=0$ the matrix $D_{\alpha\beta}^{S}+D_{\alpha\beta}^{C}$ is such that there is no coupling of the y components of the ionic displacements with the x and z components. Thus, the y-polarized normal modes are obtained by diagonalizing the 14×14 matrix $D_{yy}^{S}+D_{yy}^{C}$. The remaining 28×28 matrix, $D_{\alpha\beta}^{S}+D_{\alpha\beta}^{C}$ with $\alpha, \beta=x, z$, yields those normal modes for which the ionic displacements lie in the xz plane. Since the most interesting behavior occurs in the xz-polarized modes we shall discuss them in some detail first and then give a more brief discussion of the y-polarized modes.

For the sake of completeness, all 28 of the xz-polarized modes of a seven-layer slab are shown in Fig. 3. In this and all following plots of normal modes, the frequency is plotted versus the dimensionless variable $Q=q_x a/2\pi$, $Q=0.5$ corresponding to the zone boundary. Due to the reflection symmetry of the slab, the eigenvectors of all normal modes have definite parities with respect to the center layer of the slab. Letting l_3 and $\tilde{l}_3$ denote atomic planes equidistant from the central plane $(l_3+\tilde{l}_3=N-1)$, an even-parity mode is one whose ionic displacements satisfy

$$w_{xj}(\tilde{l}_3)=w_{xj}(l_3)\,,\quad w_{yj}(\tilde{l}_3)=w_{yj}(l_3)\,,\quad w_{zj}(\tilde{l}_3)=-w_{zj}(l_3)\,, \qquad (9.1)$$

and an odd-parity mode is one whose ionic displacements satisfy

$$w_{xj}(\tilde{l}_3)=-w_{xj}(l_3)\,,\quad w_{yj}(\tilde{l}_3)=-w_{yj}(l_3)\,,\quad w_{zj}(\tilde{l}_3)=w_{zj}(l_3)\,. \qquad (9.2)$$

The complicated behavior of the normal modes of Fig. 3 is due to the interactions of modes whose eigenvectors are of like parity. As the frequencies of two such modes approach one another they do not cross but tend to "repel" each other and their eigenvectors exchange character. Although this effect is not easily seen in Fig. 3 because of the large number of modes drawn in this figure, it is apparent

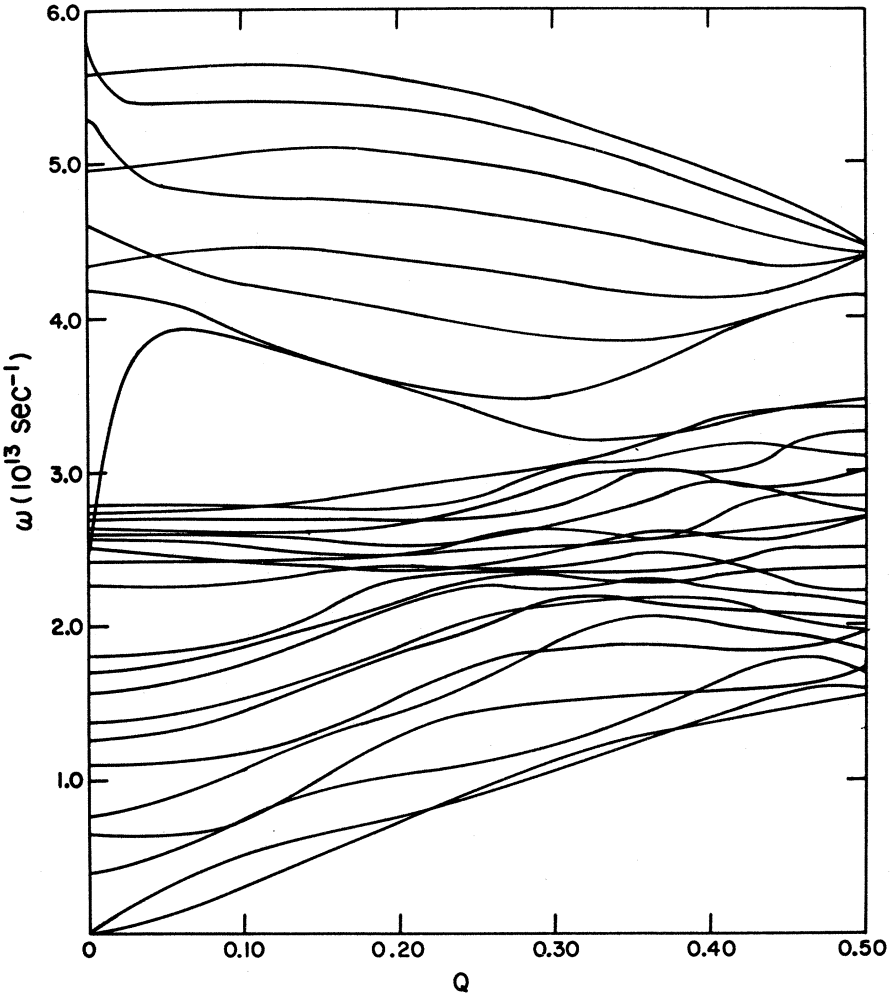

FIG. 3. Dispersion relations for xz-polarized modes of a 7-layer NaCl slab.

in Fig. 5, which we shall discuss shortly.

Of the 28 normal modes shown in Fig. 3, seven are longitudinal optical (LO), seven are transverse optical (TO), seven are longitudinal acoustical (LA), and seven are transverse acoustical (TA) modes.[14] At $Q=0$, the seven uppermost modes in the figure are the LO modes but, other than these, one cannot easily point out the other groups of modes because the LA modes cover such a wide range of frequencies that they are mixed in with the TA and TO modes.

In Fig. 4 we have plotted the frequencies of the xz-polarized optical modes for Q ranging from 0 to 0.10. The upper seven modes are longitudinal and the lower seven are transverse modes. The two transverse modes drawn in dashed lines are optical surface modes.

Looking at the LO modes at $Q=0$ in Fig. 4, the highest-frequency mode is an odd-parity mode, the second highest is even parity, and they continue to alternate in parity down to the lowest-frequency longitudinal mode, which is of odd parity. The transverse modes follow the same alternating pattern at $Q=0$ with the highest being of even parity and the two nearly degenerate surface modes being of opposite parities.

All of the LO modes, with one exception to be discussed below, are bulk modes, the uppermost one having a frequency $\omega = 5.789\times10^{13}$ sec^{-1} at $Q=0$. The uppermost mode corresponds roughly to the $\vec{q}=0$ LO mode of an infinite NaCl crystal of point ions having frequency

$$\omega = \omega_{\mathrm{LO}} = \left[\frac{e^2}{2r_0^3}\left(\frac{1}{m_+}+\frac{1}{m_-}\right)\left(A+2B+\frac{8\pi}{3}\right)\right]^{1/2}$$

$$= 5.856\times10^{13}\ \mathrm{sec}^{-1}\ . \qquad (9.3)$$

Of the five TO bulk modes, the lowermost one[15] has a frequency $\omega = 2.512\times10^{13}$ sec^{-1} at $Q=0$ and corresponds roughly to $\vec{q}=0$ TO mode of an infinite crystal for which

$$\omega = \omega_{\mathrm{TO}} = \left[\frac{e^2}{2r_0^3}\left(\frac{1}{m_+}+\frac{1}{m_-}\right)\left(A+2B-\frac{4\pi}{3}\right)\right]^{1/2}.$$

$$= 2.488\times10^{13}\ \text{sec}^{-1}\ . \qquad (9.4)$$

Of the two TO surface modes, the one whose frequency increases rapidly as Q increases from zero is of even parity and appears to correspond to the low-frequency surface mode found by Fuchs and Kliewer.[1] However, unlike their result, this surface mode remains localized at the surface in the $\vec{q}\to 0$ limit as does the odd-parity surface mode for which they found no corresponding mode. For simplicity, the even-parity surface mode has been shown crossing all of the TO bulk modes above it in the region near $Q=0$ in Fig. 4. The true behavior of these modes is as shown in Fig. 5, which is an expanded drawing of that small region of Fig. 4. Only the even-parity TO modes are shown in Fig. 5 since the odd-parity modes are unaffected in this region. At $Q=0$ the lowest-frequency mode ($\omega = 2.418\times10^{13}\ \text{sec}^{-1}$) shown is localized at the surfaces of the slab; in the region $0.0005 \lesssim 0 \lesssim 0.005$ none of the modes shown have a definite surfacelike character because of the interactions occurring in this region. Beyond $Q=0.005$ the highest-frequency mode begins to regain this surfacelike character as its frequency increases away from the other modes and the three remaining modes are then bulk modes, the eigenvectors of each now having the character of the $Q=0$ eigenvector of the mode which was directly above it at $Q=0$.

In view of this behavior of the even-parity TO surface mode, we now return to Fig. 4 and examine the LO modes more closely, keeping in mind that Fuchs and Kliewer also found an upper surface mode in their calculations. Concentrating on just the odd-parity LO modes, we see that there are interactions between these modes similar to those seen in the TO modes. Since the LO modes cover a greater range of frequencies than do the TO modes, these interactions are necessarily spread over a greater frequency and wave vector than are the TO mode interactions. Yet there is a definite indication in Fig. 4 that the uppermost mode at $Q=0(\omega\simeq\omega_{LO})$ is trying to make its way down in frequency through the other LO modes as Q increases. The range of

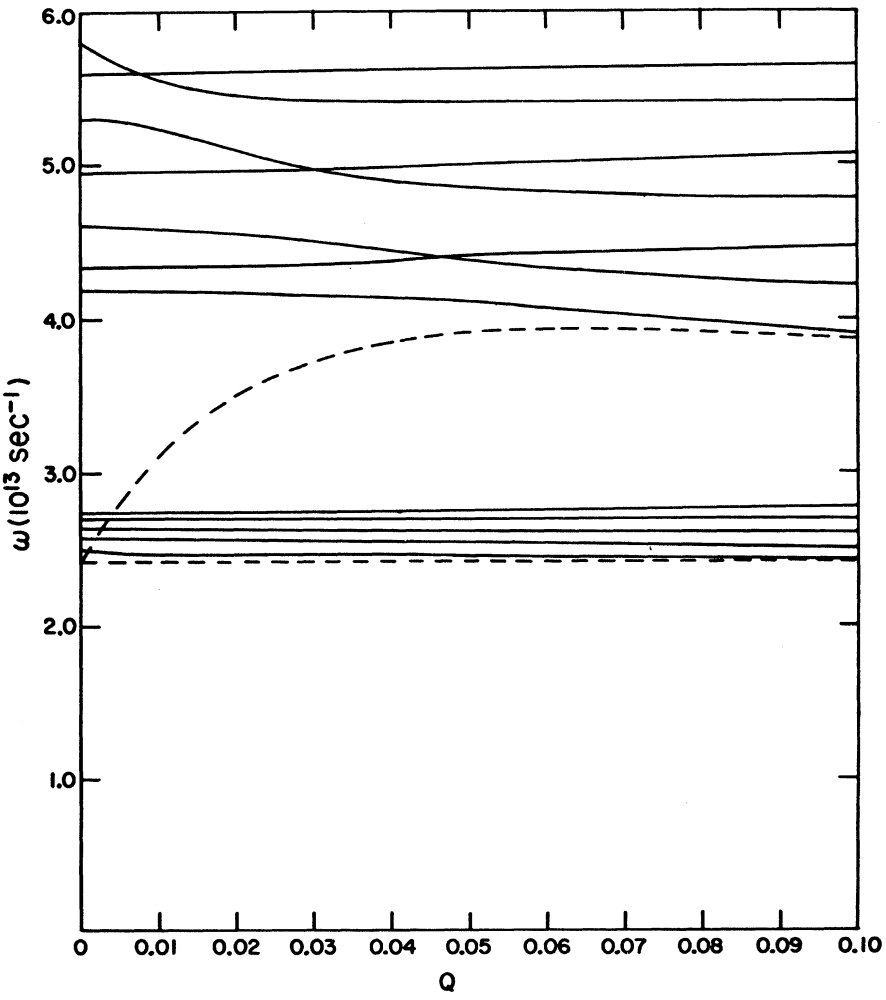

FIG. 4. Dispersion relations for xz-polarized optical modes.

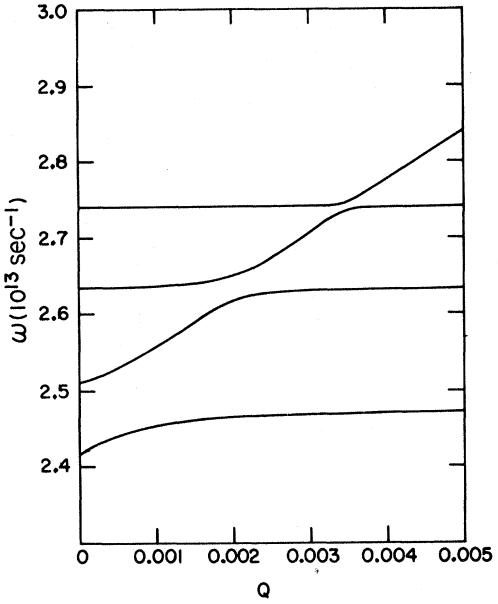

FIG. 5. Dispersion relations for even-parity xz-polarized TO modes.

frequencies of the LO modes is just too great to allow this mode to emerge well below the frequency of the lowest LO mode; nevertheless, in the range $0.1 \lesssim Q \lesssim 0.2$, the mode tends to assume a surface-like character as predicted by Fuchs and Kliewer.

In order to demonstrate this effect more clearly, the normal modes have been recalculated with the electronic charge occurring in the Coulomb matrix elements multiplied by a factor of 1.26. This was done to provide a larger gap in frequency between the LO and TO modes so that the LO surface mode might be able to emerge below the other LO modes. The odd-parity LO modes and the even-parity TO surface mode resulting from this calculation are shown in Fig. 6 as solid lines. The two dashed lines in this figure are the two surface modes calculated from the theory of Fuchs and Kliewer with e replaced by $1.26e$ and

$$\omega_0 = \left[\frac{e^2}{2r_0^3}\left(\frac{1}{m_+}+\frac{1}{m_-}\right)(A+2B)\right]^{1/2}$$

$$= 3.944\times10^{13}\ \text{sec}^{-1}\ . \qquad (9.5)$$

The lowest-frequency LO mode in the figure begins to become localized at the surfaces approximately at $Q = 0.04$ and is definitely a surface mode at $Q = 0.10$. The figure shows good qualitative agreement with the theory of Fuchs and Kliewer.

Also, in order to investigate the behavior of the optical surface modes at $Q = 0$ more closely, the normal modes of the slab were calculated with those matrix elements representing the forces acting on the surface ions being replaced by the values of those for the ions in the bulk of the crystal. By so neglecting the changes in the forces acting on the surface ions, the present theory more closely parallels that of Fuchs and Kliewer[1] in the long-wavelength region, but the two theories are still not completely equivalent. It was found that the dependence of the normal-mode frequencies on Q was changed only slightly but there were no modes localized at the surface at $Q = 0$. This agrees with the results of Fuchs and Kliewer. The lowest-frequency TO mode at $Q = 0$ is of even parity and occurs at $\omega = 2.496\times10^{13}$ sec^{-1}, very near $\omega = \omega_{TO}$. At larger values of Q, this mode appears above the other TO modes and is localized at the surfaces as in the case where the proper surface matrix elements are used. The lowest-frequency odd-parity TO mode at $Q = 0$ occurs at $\omega = 2.525\times10^{13}$ sec^{-1}; its frequency decreases slightly with increasing Q out to $Q = 0.10$ and it does become localized at the surfaces of the slab. This behavior of the odd-parity mode does not occur in the theory of Fuchs and Kliewer.

A calculation of the xz-polarized optical modes was also made for a 13-layer slab for values of Q ranging from 0 to 0.05 in steps of 0.01. The odd-parity LO modes and the even-parity TO surface mode resulting from this calculation are shown in Fig. 7. The behavior of these modes is similar to that of the modes of a seven-layer slab except that the TO surface mode is seen to rise to its maximum frequency more rapidly with increasing Q. This effect also agrees with the theory of Fuchs and Kliewer.[1] In this case the upper LO mode occurs at $\omega = 5.837\times10^{13}$ sec^{-1} at $Q = 0$ which is to be compared to $\omega_{LO} = 5.856\times10^{13}$ sec^{-1} and the lower TO bulk mode occurs at $\omega = 2.492\times10^{13}$ sec^{-1} at $Q = 0$ which is to be compared to $\omega_{TO} = 2.487\times10^{13}$ sec^{-1}. Thus the $Q = 0$ frequencies of these modes are seen to approach ω_{LO} and ω_{TO} as the slab thickness increases. Both TO surface modes occur at $\omega = 2.419\times10^{13}$ sec^{-1} at $Q = 0$, a negligible change from the seven-layer slab.

When the slab thickness increases from 7 to 13 layers, there is a qualitative change in the lowest even-parity TO bulk mode. This mode, for seven layers, is the lowest solid line in Fig. 4, or the lowest line in Fig. 5 to the right of the crossing region ($Q \gtrsim 0.003$); it is not shown in Fig. 7 for 13 layers. The mode is a bulk mode for the thinnest slab, but gradually changes to a surface mode as the thickness increases.

The change occurs in the following way. Let us consider the x-displacement amplitudes of a given atom type as a continuous function of distance across the slab, and examine where the nodes of the displacement amplitude are located. (For small Q, the displacement amplitudes for the xz-polarized TO

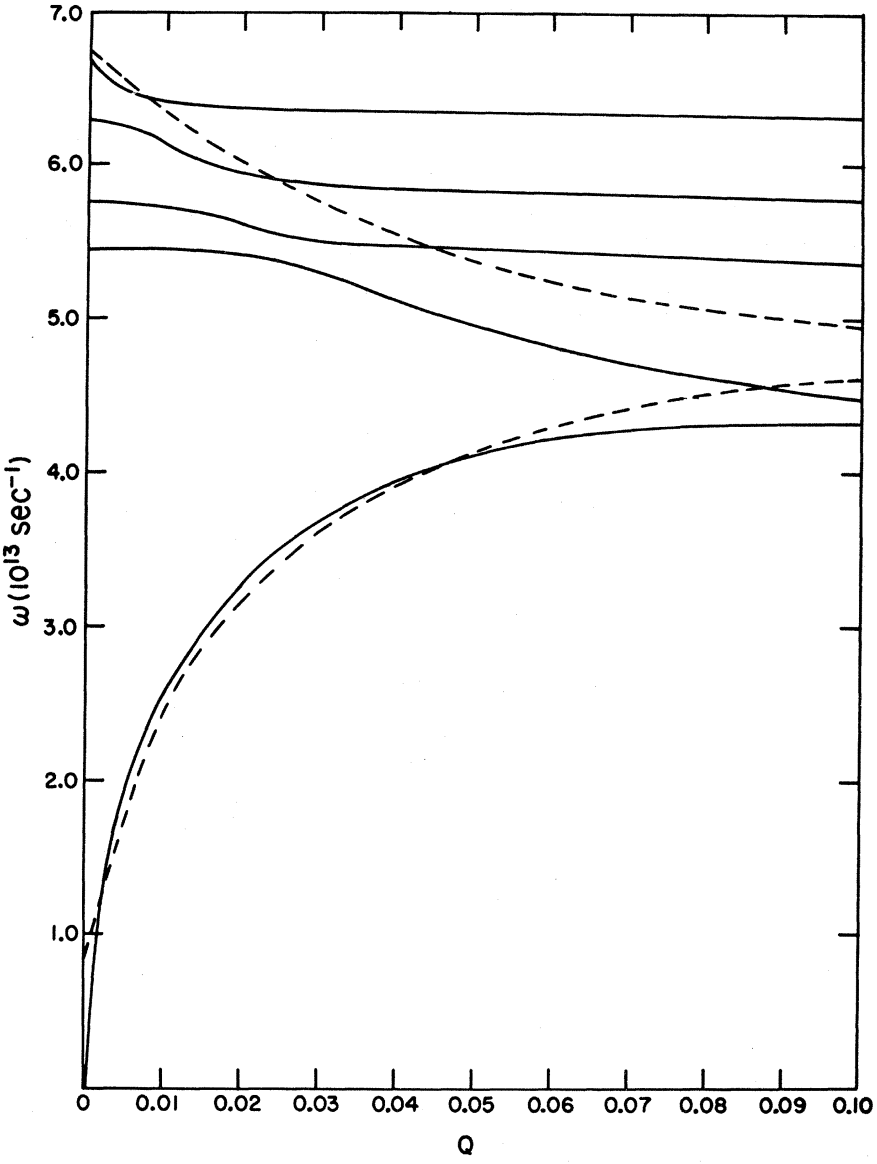

FIG. 6. Dispersion relations for odd-parity LO modes and the even-parity TO surface mode with e replaced by $1.26e$. Dashed lines are surface modes calculated from theory of Fuchs and Kliewer (see Ref. 1).

modes are very nearly in the x direction; they are exactly in the x direction at $Q=0$.) Referring to Fig. 5, where only the even-parity modes are shown, the four modes at $Q=0$, in order of increasing frequency, have 0, 2, 4, and 6 nodes, whereas at $Q=0.005$ they have 2, 4, 6, and 0 nodes, again in order of increasing frequency. At $Q=0.005$, the mode of interest, with two nodes, has many characteristics of a bulk mode: The nodes are about one atomic layer from the surfaces, and the displacement amplitude is approximately a sinusoidal function of distance across the slab. However, the amplitude is higher at the surfaces than at the center by about 30%, so the mode also has some characteristics of a surface mode. As the slab thickness increases, the two nodal points move apart, remaining at roughly the same distance from the surfaces. Moreover, the amplitude remains large at the surfaces but becomes smaller between the nodes, so that for 13 layers, the surface amplitude is about three times the central amplitude. For a very thick slab, finally, the two nodes are still near the surfaces, the central amplitude is exceedingly small, and the mode becomes very nearly degenerate with the odd-parity surface mode having a single node at the center of the slab (lower dashed line in Fig. 4). This behavior with increasing slab thickness is consistent with the requirement that the mode be orthogonal to the nodeless TO surface mode (upper dashed line in Fig. 4), which has essentially a constant amplitude across the slab just after emerging from the region near $Q=0$ where it inter-

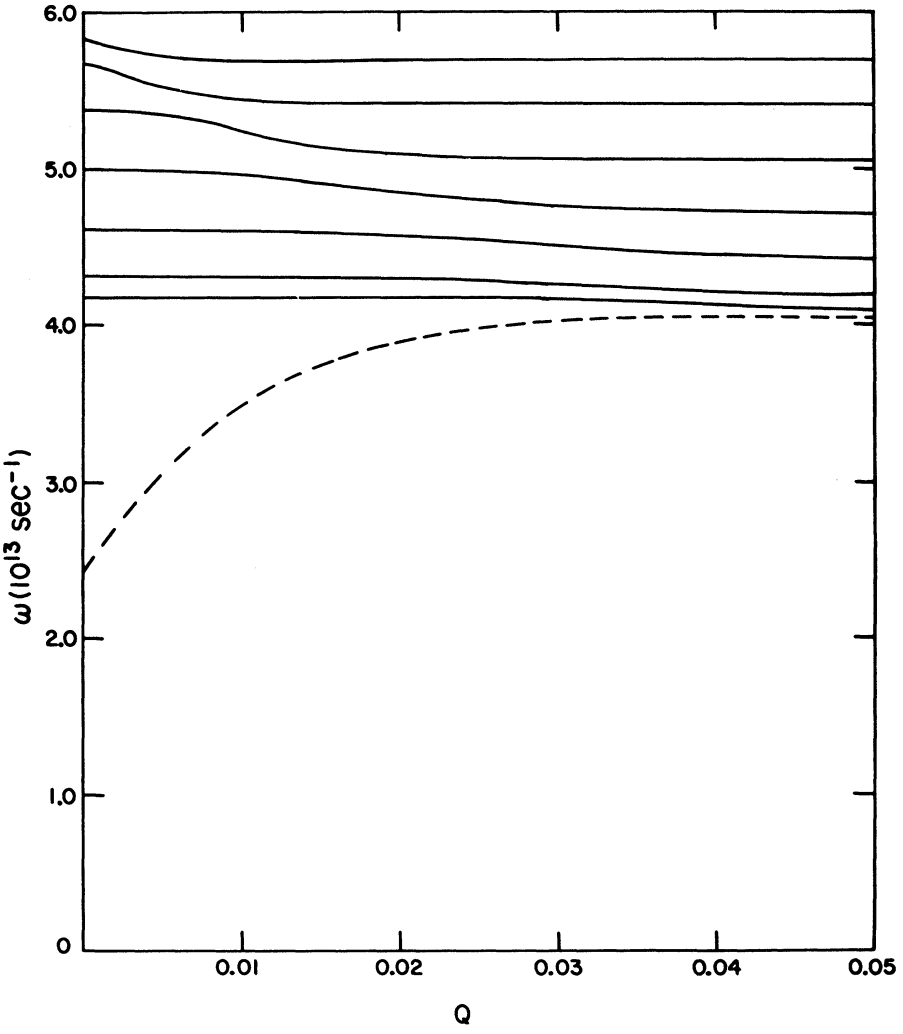

FIG. 7. Dispersion relations for odd-parity LO modes (solid lines) and the even-parity TO surface mode (dashed line) of a 13-layer NaCl slab.

acts with the bulk modes.

It is also of interest to inquire more closely about the fate of the low-frequency surface mode of Fuchs and Kliewer, which we shall denote as the "FK mode," in the $Q = 0$ limit. We stated that the even-parity TO surface mode at $Q = 0$ appears to correspond to the FK mode; this is also implied in Fig. 4, where the FK mode (upper dashed line) has been drawn so that at $Q = 0$ it goes to the frequency of the even-parity TO surface mode. However, it will be seen below that this question cannot be answered unambiguously.

The FK mode actually can be identified only where its frequency is higher than that of the TO bulk modes; it is an even-parity nodeless mode with a displacement amplitude which becomes uniform across the slab as Q decreases. When Q becomes so small that the FK mode attempts to cross the even-parity bulk modes, it loses its identity because of interactions with these modes. The problem is, then, to decide what characteristic of the FK mode is propagated through the bulk-mode region. This is where the ambiguity arises.

One might regard the nodeless character of the FK mode as its significant feature. This nodeless character is passed from one mode to the next in the region of interaction in such a way that a given bulk mode tends to be nodeless where its slope is greatest, until finally at $Q = 0$ the lowest TO surface mode is nodeless. Alternatively, one might examine how the slope $d\omega/dQ$ of a mode in the interaction region compares with that of the FK mode. The calculation for seven layers, shown in detail in Fig. 5, indicates that both the even-parity TO surface mode and the lowest even-parity TO bulk mode (i.e., the lowest and next-to-lowest lines in Fig. 5) have nonvanishing slopes at $Q = 0$. The slope of the surface mode is greater than that of the bulk mode, and also agrees more closely with the slope of the FK mode. By both of these criteria one would conclude that the FK mode becomes the TO surface mode at $Q = 0$. A third procedure might be to make

a linear extrapolation of the FK mode to see what frequency it goes to at $Q=0$. Figure 5 shows that at $Q=0$ it goes to the frequency of the lowest bulk mode rather than the surface mode. The significance of this "extrapolation criterion" is uncertain.

Calculations for a 13-layer slab show that as Q decreases, the nodeless character of the FK mode is again passed from one mode to another and finally appears at $Q=0$ in the even-parity TO surface mode, as it does for the seven-layer slab. Again, both the TO surface mode and the lowest TO bulk mode have nonvanishing slopes at $Q=0$, but now the slope of the bulk mode is greater than that of the surface mode, and it agrees more closely with that of the FK mode. Not only does the even-parity TO surface mode have a small initial slope, but it has a smaller total increase in frequency, thus remaining more nearly degenerate with the odd-parity TO surface mode (not shown in Fig. 5). The two criteria now lead to different conclusions. We believe that the number of nodes has little physical significance in this case. The even-parity TO surface mode is nodeless at $Q=0$, but the displacement amplitude of this mode is so small over most of the interior of the slab that an exceedingly small perturbation can change the sign of the amplitude at the center, introducing two nodes. The two nodes in the lowest even-parity bulk mode are between the first and second atomic layers from each surface, so a very small perturbation can move these nodes "outside" the slab, making the mode nodeless. For this reason the final transfer of the nodeless character from the bulk mode to the surface mode, which occurs as $Q\to 0$, is relatively unimportant.

We conclude tentatively that the FK mode neither becomes entirely the lowest bulk mode nor the surface mode as $Q\to 0$, but that both modes are involved. For a very thin slab the surface mode is involved to a greater extent than the lowest bulk mode, whereas the reverse is true for a thick slab.

We now turn our attention to the y-polarized modes of a seven-layer slab. There are seven TO y-polarized modes and seven TA y-polarized modes. Of each type, two are surface modes and five are bulk modes. In Fig. 8 the upper pair of solid lines are the uppermost and lowermost TO bulk modes and the lower pair of solid lines are the uppermost and lowermost TA bulk modes. The three remaining bulk modes of either type are not shown in the figure but remain at frequencies intermediate to these pairs from $Q=0$ out to $Q=0.50$, the first zone boundary. The upper dashed line in the figure represents two nearly degenerate TO surface modes of opposite parities. Although both of these modes are strongly localized at the surfaces at $Q=0$, as Q increases toward the zone boundary the surfacelike character of both becomes rather ill defined. The lower pair of dashed lines are two TA surface modes of opposite parity, the lowest one occurring at $\omega=0$ at $Q=0$ and being of even parity. Neither of these modes is localized at the surfaces at $Q=0$; the lowest one corresponds to uniform translation of the slab. They do become surfacelike in character with increasing Q, although not markedly so.

Before comparing the results of the present work to those of Lucas,[2] Tong and Maradudin,[3] and Chen

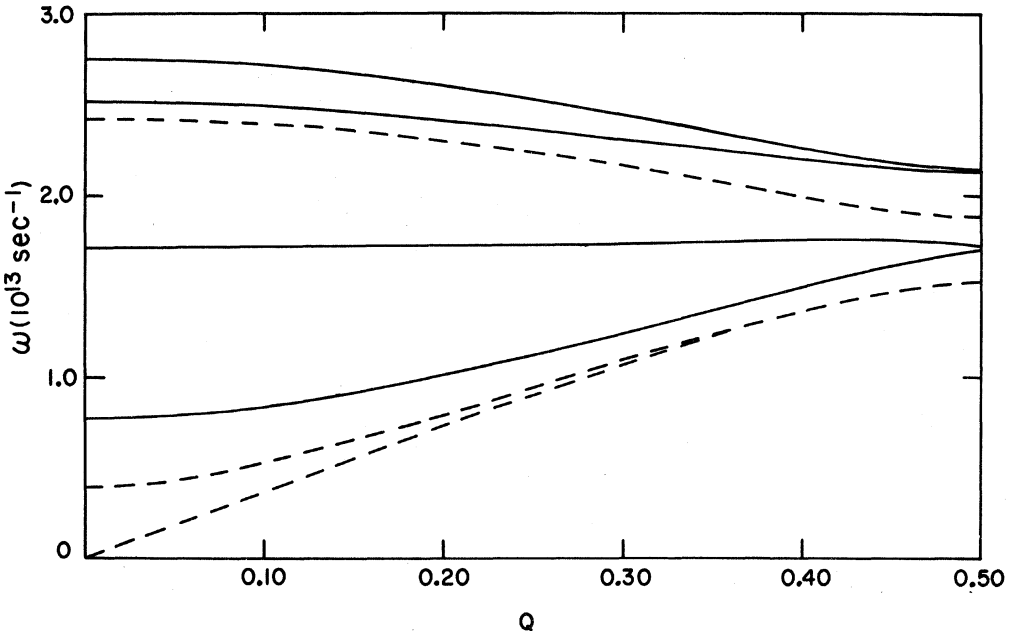

FIG. 8. Dispersion relations for y-polarized modes of a 7-layer NaCl slab.

et al.,[4] we should point out that, in view of the present theory, Tong and Maradudin's criticism of the long-wavelength approximation used by Fuchs and Kliewer does not seem to be totally correct. In their expressions for the matrix elements of the Coulomb interaction, $D^C_{\alpha\beta}(\vec{q}; l_3, l_3'; j, j')$, they correctly noted that the $m = n = 0$ terms in their sums, which are the same as the $\vec{G} = 0$ terms in the expressions presented in this paper and the integral expressions used by Fuchs and Kliewer, vanish as $\vec{q} \to 0$ while the remaining terms in the sums gives a finite result. They contended that the theory of Fuchs and Kliewer was therefore not valid for small values of $\vec{q}$ since their integral expressions did not contain the other $\vec{G} \neq 0$ terms of the sums. However, in Sec. V of this paper we have pointed out that, for a uniformly polarized infinite crystal, these $\vec{G} \neq 0$ terms are simply the Lorentz local field correction, $(4\pi/3)\vec{P}$, which Fuchs and Kliewer do include in their theory. The exponential dependence on $|l_3 - l_3'|$ of these local field terms of the dynamical matrix is such that, for long-wavelength oscillations within the slab, the local field correction differs significantly from $\frac{4}{3}\pi\vec{P}$ only at those ion sites in the surface layers of the slab. Thus, by taking the local field correction to be $\frac{4}{3}\pi\vec{P}$ for all layers of the slab, Fuchs and Kliewer did include all terms of the sums appearing in the expressions for $D^C_{\alpha\beta}(\vec{q}; l_3, l_3'; j, j')$ in their long-wavelength approximation. They simply neglected any changes occuring in these terms for ions on the surfaces of the slab in the same way that they neglected any changes in the short-range forces contained in $D^S_{\alpha\beta}(\vec{q}; l_3, l_3'; j, j')$.

The results of Lucas, Tong and Maradudin, Chen *et al.*, and the present work are all in agreement as to the number and types of optical modes which are localized at the surface at $Q = 0$. That is, there are no LO surface modes and four TO surface modes. Of these four, the eigenvectors of two are polarized in the x direction and of opposite parity and the other two are identical except that their eigenvectors are polarized in the y direction. None of the modes found by Fuchs and Kliewer were localized at the surfaces at $Q = 0$. The present theory indicates that this is indeed due to their neglect of the changes in the forces acting on surface ions, as suggested by Lucas. A calculation of the y-polarized modes from the present theory with the matrix elements for the surface ions set equal to those for the bulk ions yield no y-polarized surface modes of any type for all values of Q, indicating that this same reason is also responsible for the fact that Fuchs and Kliewer found no y-polarized surface modes.

For values of Q different from zero, several discrepancies between the results of the present work and those of Tong and Maradudin[3] appear. Tong and Maradudin report a total of six optical surface modes occurring in three nearly degenerate pairs represented by the three dashed lines in Fig. 9. The two lower pairs, labeled by (b) and (c) in the figure, are transverse, while the polarization of the upper pair, (a), is not reported. Also the displacement amplitudes of the upper pair are reported to have very little attenuation at the point $Q = 0$.

The two surface modes (a) appear to correspond to the TO and LO surface modes we find in the same frequency range. As Q (or k_x) $\to 0$, we find that the two modes separate, one mode passing down through the TO bulk modes, the other passing up through the LO bulk modes. Tong and Maradudin chose their x axis along a [100] direction rather than a [110] direction as in the present work; this would certainly affect the modes for large values of Q but should not alter their qualitative behavior at small values of Q. Their reported results were calculated for $q_y = 0$ and $q_x = 0.2n\pi/r_0$ with $n = 0$, 1, 2, 3, 4, and 5, $q_x = \pi/r_0$ being the first zone boundary along their x axis. Their first nonzero $q_x = 0.2\pi/r_0$ corresponds to a value of our $Q = \frac{1}{2} q_x a/\pi = \sqrt{\frac{1}{2}}\, q_x r_0/\pi = 0.14$. This rather coarse mesh of values of q_x might be responsible for the reported absence of any splitting of the modes (a) as $q_x \to 0$. At $q_x = 0$ we find no modes corresponding to their modes (a).

The two surface modes (b) correspond to our odd-parity TO surface mode and our lowest-frequency even-parity TO bulk mode. Tong and Maradudin carried out their calculations for a 15-layer slab, whereas our calculations are for a seven-layer slab. Since we have seen above that this particular bulk mode changes to a surface mode as the slab thickness increases, such an assignment is, in fact,

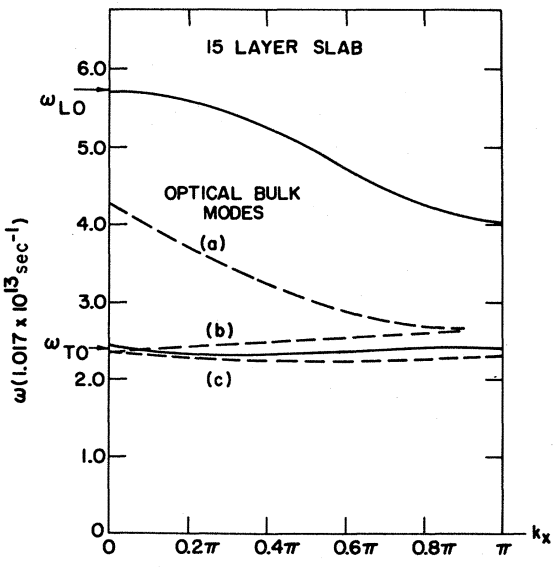

FIG. 9. Dispersion relations of optical modes of a 15-layer NaCl slab as reported by Tong and Maradudin (see Ref. 3). Here $k_x = q_x r_0 = \pi Q\sqrt{2}$.

consistent. Finally, the two modes (c) agree with our TO y-polarized surface modes.

Chen *et al.*,[4] have calculated the normal modes of an ionic-crystal slab containing 15 atomic layers. Because of the greater number of layers, they find more bulk modes and report one more surface mode in the region immediately below the bulk modes than we do; otherwise their results generally agree with ours. They find additional surface modes near the edges of the Brillouin zone, in regions of $\vec{q}$ space which we do not examine. On the other hand, we investigate the details of the modes near $\vec{q}=0$ more thoroughly. For example, they do not report the crossing near $\vec{q}=0$ of even- and odd-parity LO modes, as we show in Figs. 3 and 4; presumably their mesh of $\vec{q}$ values is too coarse to see the crossing.

No calculations of the normal modes of the slab including retardation were made in this work. Since the elements of the dynamical matrix depend on ω in this case, one cannot use a simple diagonalization procedure to calculate the normal-mode eigenfrequencies and eigenvectors. However, the fact that the dynamical matrix is found to be Hermitian for $q>\omega/c$ and non-Hermitian for $q<\omega/c$ is in agreement with the existence of nonradiative and radiative modes as found by Kliewer and Fuchs.[5] Also the structure of the retarded dynamical matrix D^C is such that only the $\vec{G}=0$ terms, i.e., the macroscopic electric field, is changed significantly by the inclusion of retardation and this change is greatest in the region $|\vec{q}|\lesssim\omega/c$.

In comparing our work to that of Bryksin and Firsov,[6] we note that although 24 surface modes were not found in the present work, we do find that two distinct types of surface modes occur depending upon whether or not the changes in the short-range forces acting on surface ions are included in the theory. Inclusion of these changes results in modes which are strongly localized at the surfaces for $\vec{q}\simeq 0$, and exclusion of these changes results in weakly localized surface modes for small $\vec{q}$. There is no indication in the present work that the two types exist separately for $q\simeq 0$ and then merge as q increases as suggested by Bryksin and Firsov. Their conclusion concerning the validity of the dielectric constant formalism used by Fuchs and Kliewer is supported by the present work except for the interactions which we found to occur between surface and bulk modes. The effects of these interactions are not included in the theories of either Bryksin and Firsov or Fuchs and Kliewer.

X. OPTICAL PROPERTIES

The transmittance, reflectance, and absorptance of a NaCl crystal slab of 15 layers have been calculated using the theory given in Sec. III. The calculations were made for both P and S polarizations of the electric field with an angle of incidence of 75 degrees and a damping constant $\gamma=5.0\times10^{11}$ sec^{-1}. (This choice of γ will be discussed later.) The absorptance is plotted as a function of frequency for the case of P polarization in Fig. 10, and for the case of S polarization in Fig. 11.

The frequency range 2.2×10^{13} sec$^{-1}\leq\omega\leq6.0\times10^{13}$ sec^{-1} shown in Fig. 10 includes the $\vec{q}=0$ frequencies of all optical modes of vibration.[16] Outside this region the absorptance becomes very small and will not be discussed here. All absorptance peaks shown in Fig. 10 arise from the xz-polarized optical modes. The absorptance peak occurring at $\omega=2.42\times10^{13}$ sec^{-1} arises from the even-parity TO surface mode which occurs at that frequency and is seen to be comparable in size to the neighboring peak at $\omega=2.49\times10^{13}$ sec$^{-1}\cong\omega_{\mathrm{TO}}$, which is the frequency of the lowest TO bulk mode. The absorptance peaks due to the other even-parity TO bulk modes are not visible with the value of γ chosen. Each of the eight peaks which occur in the range 4.0×10^{13} sec$^{-1}\leq\omega\leq6.0\times10^{13}$ sec^{-1} arises from one of the eight odd-parity LO modes of the 15-layer slab. The largest peak occurs at $\omega=5.84\times10^{13}$ sec$^{-1}=\omega_{\mathrm{LO}}$, which is the frequency of the highest LO mode.

For the case of S polarization, peaks in the absorptance occur only at $\omega=2.42\times10^{13}$ and 2.49×10^{13} sec^{-1}. These peaks arise from the even-parity y-polarized TO surface mode and the lowest-frequency y-polarized TO bulk mode, respectively. For S polarization, the electric field vector is in the y direction and does not interact with the xz-polarized modes. Thus there are no peaks and the absorptance is small for $\omega\gtrsim2.8\times10^{13}$ sec^{-1}.

The transmittance and reflectance are not shown for either polarization because the reflectance is very small for this thin slab. A plot of $1-T$ would differ significantly from the given plot of A only near the large peak occurring at $\omega=5.85\times10^{13}$ sec^{-1} for P polarization; here the reflectance reaches its maximum value of 1.12×10^{-2}.

These same optical properties of a 15-layer slab were also calculated using the local approximation of Sec. VIII with $\gamma=5.0\times10^{11}$ sec^{-1}. There was no significant difference between these results and those of the nonlocal theory. Various values of γ were tried in both the local and nonlocal calculations and no significant differences were found for any reasonable value of γ.

The experiments of Haas[17] and Jones *et al.*[18] indicate that a reasonable choice for a frequency-independent damping constant should be in the range $10^{11}\lesssim\gamma\lesssim10^{12}$ sec^{-1} for temperatures in the range $0<T\lesssim300\,^{\circ}$K. Although the location in frequency of the absorption peaks does not depend on the value of γ chosen, they do become sharper and reach a higher maximum as γ decreases.

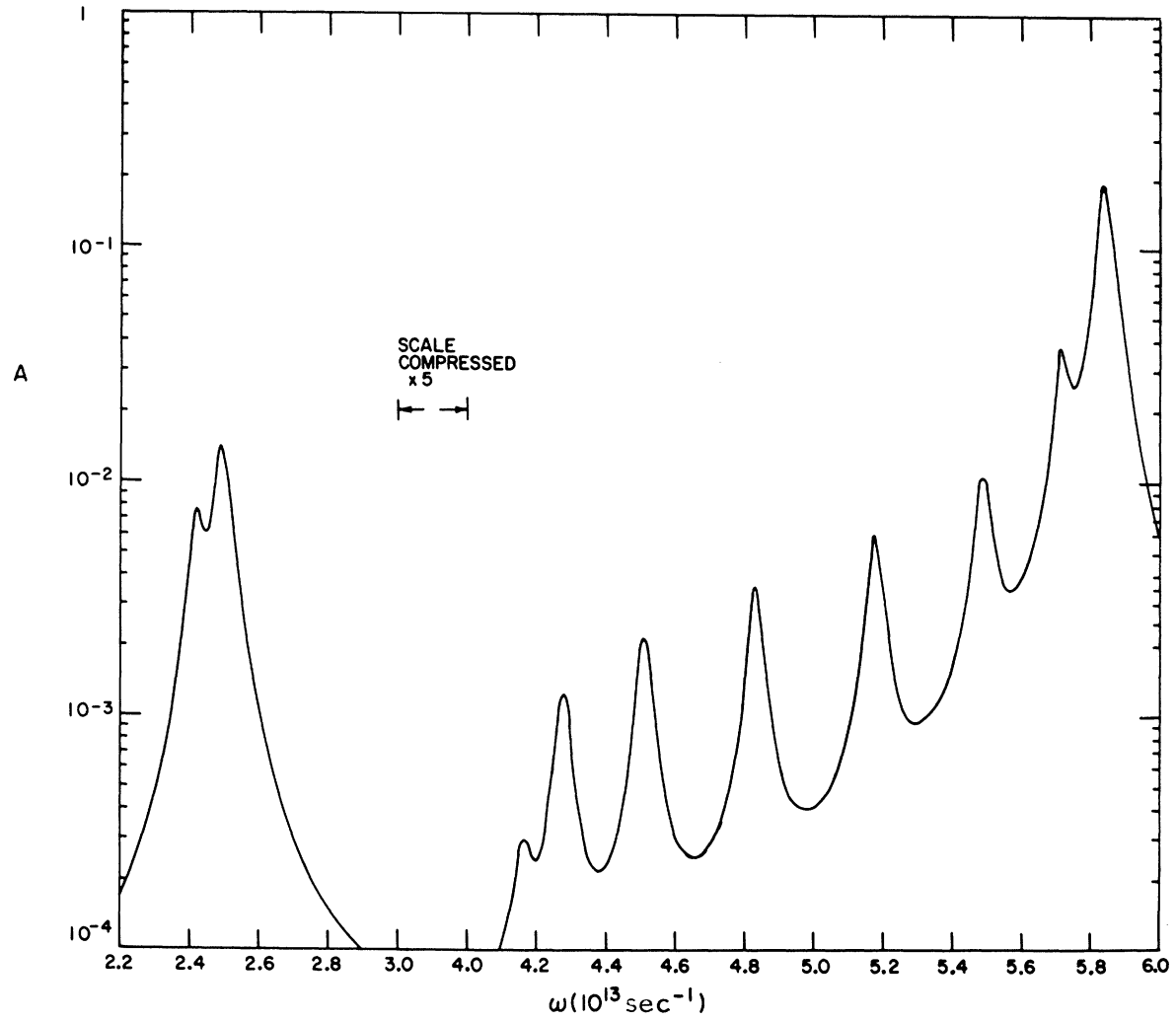

FIG. 10. Absorptance as a function of frequency for P-polarized light incident at an angle of 75° on a 15-layer NaCl slab.

In their work, Tong and Maradudin[3] calculated the imaginary part of the local dielectric response tensor $\epsilon^{(2)}_{\mu\nu}(\omega)$, which has peaks at the same frequencies as the absorptance. Their calculation was made for a 15-layer NaCl slab with no intrinsic damping ($\gamma = 0$). The frequencies and relative sizes of the peaks in $\epsilon^{(2)}_{\mu\nu}(\omega)$ reported by them agree fairly well with the absorption spectra found in the present work except that they reported no peak in $\epsilon^{(2)}_{zz}(\omega)$ at $\omega = 4.16\times10^{13}$ sec^{-1} corresponding to the peak which arises from the lowest-frequency odd-parity LO mode in the present work. They also report two small peaks in $\epsilon^{(2)}_{xx}(\omega)$ at $\omega \simeq 2.52\times10^{13}$ and 2.62×10^{13} sec^{-1} which presumably arise from TO bulk modes but do not show up in the absorption spectra of the present work. The absence of any peaks arising from TO modes other than those shown in the present work is due to the value of γ chosen. (Peaks in this region start to become visible for $\gamma \lesssim 10^{11}$ sec^{-1}.)

We may also compare the results of the present theory to the calculation by Berreman[7] based on the local dielectric function $\epsilon(\omega)$ of an infinite ionic crystal. He points out that for the case of P polarization with non-normal incidence there is a component of the electric field normal to the plane of the slab and an absorption peak should therefore occur at $\omega = \omega_{LO}$ in this case. Using Maxwell's equations and matching appropriate boundary conditions at the surfaces of the slab, he has derived expressions for the transmittance and reflectance of a thin ionic-crystal slab in terms of the slab thickness, angle of incidence, and $\epsilon(\omega)$ of the crystal. He computed the transmittance of both S- and P-polarized radiation by a lithium fluoride film 0.20 μ thick. His calculations included a frequency-dependent damping term $\gamma(\omega)$ and were made for an angle of incidence of 30°. He also measured the transmit-

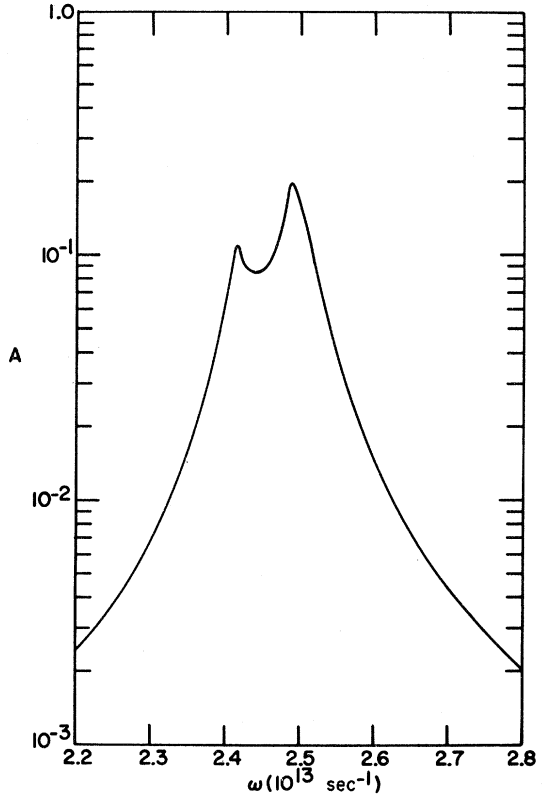

FIG. 11. Absorptance as a function of frequency for S-polarized light incident at an angle of 75° on a 15-layer NaCl slab.

tance of a 0.20-μ-thick LiF film for both polarizations of the incident field. His theoretical and experimental results are shown in Figs. 12 and 13, respectively. The dashed lines in these figures at 14.8 and 32.6 μ denote the frequencies of the LO and TO modes in an infinite crystal, ω_{LO} and ω_{TO}. From Fig. 12 we see that his calculated results for the transmittance of P polarized light (solid line) shows minima at both ω_{TO} and ω_{LO}, while for S polarization (dashed line) there is a transmittance minimum only at ω_{TO}. This result agrees with the present work. Berreman's calculation does not yield any of the other absorptance peaks found in the present theory since $\epsilon(\omega)$ contains no information about the remaining bulk and surface modes of the slab. His experimental results show good qualitative agreement with the predictions of his theory.

Although it is certainly not reasonable to attempt any quantitative comparison of Berreman's[7] experimental results to the results of the present work, we should note that all features of Fig. 13 can be qualitatively explained by the present theory. A LiF film 0.20 μ thick contains approximately 10^3 layers of ions while the calculations of the optical properties of the present theory were made for a point-ion model of a NaCl film containing 15 layers

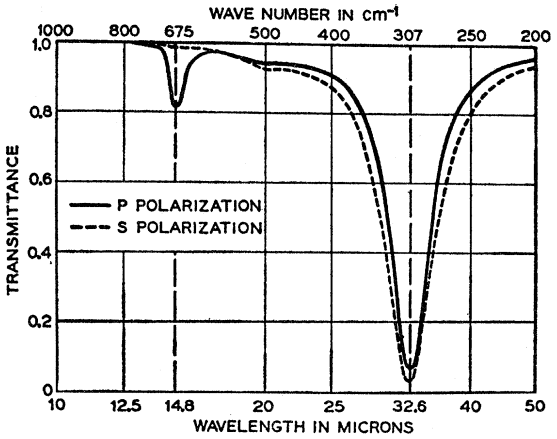

FIG. 12. Transmittance of S-polarized and P-polarized light incident at an angle of 30° on a 0.20-μ-thick LiF slab as calculated by Berreman (see Ref. 7).

of ions. From the present theory we would expect that the LiF film would have a TO surface mode at a frequency slightly below its transverse optical frequency ω_{TO}, but that the absorptance due to this surface mode should be much less than that due to the bulk mode at ω_{TO}. This agreement offers a possible explanation of the small dip in the transmittance which occurs at approximately 36 μ in Fig. 13. The fact that this dip is seen for both P and S polarizations is consistent with the assertion that it arises from a transverse mode. We would also expect, for the LiF film used by Berreman, that approximately 5×10^2 absorptance peaks arising from odd-parity LO bulk modes should occur below ω_{LO} in a range of frequencies $\Delta\omega$ of approximately the same width ($\Delta\omega \sim 2\times10^{13}$ sec^{-1}) as that occupied

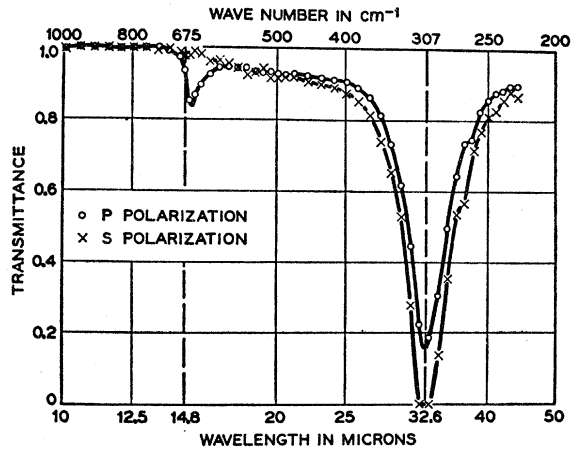

FIG. 13. Transmittance of S-polarized and P-polarized light incident in a cone from 26° to 34° on a 0.20-μ-thick LiF slab as experimentally observed by Berreman (see Ref. 7).

by those peaks shown for the 15-layer NaCl slab. (This width is determined by the bandwidth of the LO branch of an infinite crystal.) Experimentally these peaks would not be resolved, and one would expect to see a smoothly varying absorptance in this frequency range. The absorptance should gradually increase as ω increases from the frequency of the lowest LO bulk mode to ω_{LO}; it should then decrease more rapidly with increasing frequency greater than ω_{LO} since there are no modes found in that region. This behavior of the absorptance should contribute to the asymmetry of the dip in the transmittance of P polarized light at ω_{LO} in Fig. 13. This behavior is neither expected nor seen for S polarization because it is due to the excitation of LO modes. Thus the present theory offers a qualitative explanation of all of the structure exhibited by the transmittance in Fig. 13.

APPENDIX A

Here we list several representative elements of D^C for $l_3' = l_3$.

For $|q_x| > \omega/c$:

$$D^C_{xy}(\vec{q}; l_3, l_3; j, j') = D^C_{yx}(\vec{q}; l_3, l_3; j, j')$$

$$= -i\frac{2e_je_{j'}}{a(m_jm_{j'})^{1/2}} \sum_{l_y}\sum_{G_x} \frac{l_y + s_{j'y} - s_{jy}}{|l_y + s_{j'y} - s_{jy}|} (q_x+G_x) \left((q_x+G_x)^2 - \frac{\omega^2}{c^2}\right)^{1/2} e^{i(q_x+G_x)(s_{jx}-s_{j'x})}$$

$$\times K_1([(q_x+G_x)^2 - \omega^2/c^2]^{1/2} |l_y + s_{j'y} - s_{jy}|) e^{iq_yl_y}, \quad \text{(A1)}$$

$$D^C_{xy}(\vec{q}; l_3, l_3; j, j) = D^C_{yx}(\vec{q}; l_3, l_3; j, j)$$

$$= -\frac{2e_j^2}{am_j} \sum_{l_y}{}' \sum_{G_x} \frac{l_y}{|l_y|} (q_x+G_x)^2 \left((q_x+G_x)^2 - \frac{\omega^2}{c^2}\right)^{1/2} K_1([(q_x+G_x)^2 - \omega^2/c^2]^{1/2} |l_y|) e^{iq_yl_y}, \quad \text{(A2)}$$

$$D^C_{zz}(\vec{q}; l_3, l_3; j, j') = -[D^C_{xx}(\vec{q}; l_3, l_3; j, j') + D^C_{yy}(\vec{q}; l_3, l_3; j, j')]$$

$$-\frac{4e_je_{j'}}{a(m_jm_{j'})^{1/2}} \frac{\omega^2}{c^2} \sum_{l_y}\sum_{G_x} K_0([(q_x+G_x)^2 - \omega^2/c^2]^{1/2} |l_y + s_{j'y} - s_{jy}|) e^{i(q_x+G_x)(s_{jx}-s_{j'x})} e^{iq_yl_y}, \quad \text{(A3)}$$

$$D^C_{zz}(\vec{q}; l_3, l_3; j, j) = -[D^C_{xx}(\vec{q}; l_3, l_3; j, j) + D^C_{yy}(\vec{q}; l_3, l_3; j, j)] - 3i\frac{e_j^2}{m_j}\frac{\omega^3}{c^3} - 2\frac{e_j^2}{m_j}\frac{\omega^2}{c^2}\sum_{\vec{l}'}{}' \frac{e^{i(\omega/c)|\vec{l}'|}}{|\vec{l}'|} e^{i\vec{q}\cdot\vec{l}'}. \quad \text{(A4)}$$

For $|q_y| > \omega/c$:

$$D^C_{yy}(\vec{q}; l_3, l_3; j, j') = -\frac{2e_je_{j'}}{a(m_jm_j')^{1/2}} \sum_{l_x}\sum_{G_y} \left(\frac{\omega^2}{c^2} - (q_y+G_y)^2\right) e^{i(q_y+G_y)(s_{jy}-s_{j'y})}$$

$$\times K_0([(q_y+G_y)^2 - \omega^2/c^2]^{1/2} |l_x + s_{j'x} - s_{jx}|) e^{iq_xl_x}, \quad \text{(A5)}$$

$$D^C_{yy}(\vec{q}; l_3, l_3; j, j) = \frac{1}{m_j}\varphi^C_{yy}(0, 0; l_3, l_3; j, j) - \frac{2e_j^2}{am_j}\sum_{l_x}{}'\sum_{G_y}\left(\frac{\omega^2}{c^2} - (q_y+G_y)^2\right) K_0([(q_y+G_y)^2 - \omega^2/c^2]^{1/2}|l_x|) e^{iq_xl_x}$$

$$-\frac{2e_j^2}{am_j}\sum_{l_y}{}' \frac{e^{i(\omega/c)|l_y|}}{|l_y|}\left(\frac{1}{|l_y|^2} - i\frac{\omega}{c}\frac{1}{|l_y|}\right) e^{iq_yl_y}. \quad \text{(A6)}$$

APPENDIX B

Here we list the elements of D^C excluding retardation.

For $l_3 \neq l_3'$:

$$D^C_{xx}(\vec{q}; l_3, l_3'; j, j') = \frac{2\pi e_je_{j'}}{a_c(m_jm_{j'})^{1/2}} \sum_{\vec{G}} (q_x+G_x)^2 \frac{e^{-|\vec{q}+\vec{G}||l_3-l_3'|r_0}}{|\vec{q}+\vec{G}|} e^{i(\vec{q}+\vec{G})\cdot(\vec{s}_j-\vec{s}_{j'})}, \quad \text{(B1)}$$

$$D^C_{yy}(\vec{q}; l_3, l_3'; j, j') = \frac{2\pi e_je_{j'}}{a_c(m_jm_{j'})^{1/2}} \sum_{\vec{G}} (q_y+G_y)^2 \frac{e^{-|\vec{q}+\vec{G}||l_3-l_3'|r_0}}{|\vec{q}+\vec{G}|} e^{i(\vec{q}+\vec{G})\cdot(\vec{s}_j-\vec{s}_{j'})}, \quad \text{(B2)}$$

$$D^C_{zz}(\vec{q};l_3,l_3';j,j') = -[D^C_{xx}(\vec{q};l_3,l_3';j,j')+D^C_{yy}(\vec{q};l_3,l_3';j,j')], \tag{B3}$$

$$D^C_{xy}(\vec{q};l_3,l_3';j,j') = D^C_{yx}(\vec{q};l_3,l_3';j,j') = \frac{2\pi e_j e_{j'}}{a_c(m_j m_{j'})^{1/2}} \sum_{\vec{G}} (q_x+G_x)(q_y+G_y)\, \frac{e^{-|\vec{q}+\vec{G}||l_3-l_3'|r_0}}{|\vec{q}+\vec{G}|}\, e^{i(\vec{q}+\vec{G})\cdot(\vec{s}_j-\vec{s}_{j'})}, \tag{B4}$$

$$D^C_{xz}(\vec{q};l_3,l_3';j,j') = D^C_{zx}(\vec{q};l_3,l_3';j,j') = i\,\frac{2\pi e_j e_{j'}}{a_c(m_j m_{j'})^{1/2}}\,\frac{l_3-l_3'}{|l_3-l_3'|} \sum_{\vec{G}} (q_x+G_x)\, e^{-|\vec{q}+\vec{G}||l_3-l_3'|r_0}\, e^{i(\vec{q}+\vec{G})\cdot(\vec{s}_j-\vec{s}_{j'})}, \tag{B5}$$

$$D^C_{yz}(\vec{q};l_3,l_3';j,j') = D^C_{zy}(\vec{q};l_3,l_3';j,j') = i\,\frac{2\pi e_j e_{j'}}{a_c(m_j m_{j'})^{1/2}}\,\frac{l_3-l_3'}{|l_3-l_3'|} \sum_{\vec{G}} (q_y+G_y)\, e^{-|\vec{q}+\vec{G}||l_3-l_3'|r_0}\, e^{i(\vec{q}+\vec{G})\cdot(\vec{s}_j-\vec{s}_{j'})}. \tag{B6}$$

For $l_3 = l_3'$, $j \neq j'$:

$$D^C_{xx}(\vec{q};l_3,l_3;j,j') = \frac{2e_j e_{j'}}{a(m_j m_{j'})^{1/2}} \sum_{l_y}\sum_{G_x} (q_x+G_x)^2\, e^{i(q_x+G_x)(s_{jx}-s_{j'x})}\; K_0(|q_x+G_x|\,|l_y+s_{j'y}-s_{jy}|)\, e^{iq_y l_y}, \tag{B7}$$

$$D^C_{yy}(\vec{q};l_3,l_3;j,j') = \frac{2e_j e_{j'}}{a(m_j m_{j'})^{1/2}} \sum_{l_x}\sum_{G_y} (q_y+G_y)^2\, e^{i(q_y+G_y)(s_{jy}-s_{j'y})}\; K_0(|q_y+G_y|\,|l_x+s_{j'x}-s_{jx}|)\, e^{iq_x l_x}, \tag{B8}$$

$$D^C_{zz}(\vec{q};l_3,l_3;j,j') = [D^C_{xx}(\vec{q};l_3,l_3;j,j')+D^C_{yy}(\vec{q};l_3,l_3;j,j')], \tag{B9}$$

$$D^C_{xy}(\vec{q};l_3,l_3;j,j') = D^C_{yx}(\vec{q};l_3,l_3;j,j') = -i\,\frac{2e_j e_{j'}}{a(m_j m_{j'})^{1/2}} \sum_{l_y}\sum_{G_x} \frac{l_y+s_{j'y}-s_{jy}}{|l_y+s_{j'y}-s_{jy}|}$$
$$\times (q_x+G_x)|q_x+G_x|\, e^{i(q_x+G_x)(s_{jx}-s_{j'x})} K_1(|q_x+G_x|\,|l_y+s_{j'y}-s_{jy}|)\, e^{iq_y l_y}, \tag{B10}$$

$$D^C_{xz}(\vec{q};l_3,l_3;j,j') = D^C_{zx}(\vec{q};l_3,l_3;j,j') = D^C_{yz}(\vec{q};l_3,l_3;j,j') = D^C_{zy}(\vec{q};l_3,l_3;j,j') = 0. \tag{B11}$$

For $l_3 = l_3'$, $j = j'$:

$$D^C_{xx}(\vec{q};l_3,l_3;j,j) = \frac{1}{m_j}\,\Phi^{CU}_{xx}(0,0;l_3,l_3;j,j) + \frac{2e_j^2}{am_j}\sum_{l_y}{}' \sum_{G_x} (q_x+G_x)^2 K_0(|q_x+G_x|\,|l_y|)\, e^{iq_y l_y} - \frac{2e_j^2}{m_j}\sum_{l_x}{}' \frac{e^{iq_x l_x}}{|l_x|^3}, \tag{B12}$$

$$D^C_{yy}(\vec{q};l_3,l_3;j,j) = \frac{1}{m_j}\,\Phi^{CU}_{yy}(0,0;l_3,l_3;j,j) + \frac{2e_j^2}{m_j}\sum_{l_x}{}' \sum_{G_y} (q_y+G_y)^2 K_0(|q_y+G_y|\,|l_x|)\, e^{iq_x l_x} - \frac{2e_j^2}{m_j}\sum_{l_y}{}' \frac{e^{iq_y l_y}}{|l_y|^3}, \tag{B13}$$

$$D^C_{zz}(\vec{q};l_3,l_3;j,j) = -[D^C_{xx}(\vec{q};l_3,l_3;j,j)+D^C_{yy}(\vec{q};l_3,l_3;j,j)], \tag{B14}$$

$$D^C_{xy}(\vec{q};l_3,l_3;j,j) = D^C_{yx}(\vec{q};l_3,l_3;j,j) = -i\,\frac{2e_j^2}{am_j}\sum_{l_y}{}' \sum_{G_x} \frac{l_y}{|l_y|}\,(q_x+G_x)|q_x+G_x|\,K_1(|q_x+G_x|\,|l_y|)\, e^{iq_y l_y}, \tag{B15}$$

$$D^C_{xz}(\vec{q};l_3,l_3;j,j) = D^C_{zx}(\vec{q};l_3,l_3;j,j) = D^C_{yz}(\vec{q};l_3,l_3;j,j) = D^C_{zy}(\vec{q};l_3,l_3;j,j) = 0. \tag{B16}$$

---

*Work was performed in the Ames Laboratory of the U. S. Atomic Energy Commission, Contribution No. 3021.

†Present address: ASG Industries Inc., P.O. Box 929, Kingsport, Tenn. 37662.

[1]R. Fuchs and K. L. Kliewer, Phys. Rev. 140, A2076 (1965).

[2]A. A. Lucas, J. Chem. Phys. 48, 3156 (1968).

[3]S. Y. Tong and A. A. Maradudin, Phys. Rev. 181, 1318 (1969).

[4]T. S. Chen, R. E. Allen, G. P. Alldredge, and F. W. deWette, Solid State Commun. 8, 2105 (1970).

[5]K. L. Kliewer and R. Fuchs, Phys. Rev. 144, 495 (1966); 150, 573 (1966).

[6]V. V. Bryksin and Y. A. Firsov, Fiz. Tverd. Tela 11, 2167 (1969) [Sov. Phys. Solid State 11, 1751 (1970)].

[7]D. W. Berreman, Phys. Rev. 130, 2193 (1963).

[8]Tong and Maradudin (Ref. 3) found that if the ions are allowed to relax to their equilibrium positions in the slab, the qualitative behavior of the modes is not changed. The frequencies of the modes change by less than 4%; moreover, the modes tend to shift in the same direction (towards a higher frequency).

[9]E. W. Kellerman, Phil. Trans. Roy. Soc. London A238, 513 (1940).

[10]J. D. Jackson, *Classical Electrodynamics* (Wiley, New York, 1962).

[11]I. S. Gradshteyn and I. M. Ryzik, *Table of Integrals, Series and Products*, 4th ed. (Academic, New York, 1965).

[12]In these $\vec{G} \neq 0$ terms, $\vec{q}$ and ω/c are taken to be zero since they are small in comparison to any $\vec{G}$ and always appear added to $\vec{G}$.

[13]In the limit as $\vec{k} \to 0$, that part of the dynamical matrix associated with the macroscopic field, $D^M_{\alpha\beta}(\vec{k};\, l_3,\, l_3';\, j,\, j')$, vanishes when $l_3 \neq l_3'$, and is negligible when $l_3 = l_3$; it follows from Eq. (5.2) that $D^C \approx D^L$. The eigenvalues and eigenvectors of $D^S_{\alpha\beta}(0;\, l_3,\, l_3',\, j,\, j') + D^L_{\alpha\beta}(0;\, l_3,\, l_3';\, j,\, j')$, which are involved in the theory of the optical properties, are, therefore, the same as the eigenvalues and eigenvectors of the complete dynamical matrix $D^S_{\alpha\beta}(\vec{q};\, l_3,\, l_3';\, j,\, j')$

$+D^{C}_{\alpha\beta}(\vec{q}; l_3, l_3'; j, j')$ with $\vec{q}=0$.

[14]This classification of the normal modes into four types is strictly valid only at $Q=0$, but it remains approximately valid for Q as large as 0.1. For larger values of Q, many modes interact and exchange characters, so the classification is generally no longer useful.

[15]The lowermost TO bulk mode gradually assumes the character of a surface mode as the slab thickness increases. This mode will be discussed in more detail below.

[16]The optical properties are determined from the $\vec{q}=0$ unretarded normal modes (cf. Ref. 13).

[17]M. Haas, Phys. Rev. 117, 1497 (1960).

[18]G. O. Jones, D. H. Martin, P. A. Mawer, and C. H. Perry, Proc. Roy. Soc. (London) A261, 10 (1961).

PHYSICAL REVIEW B VOLUME 4, NUMBER 10 15 NOVEMBER 1971

Pyroelectric Coefficient of Lithium Sulfate Monohydrate (4.2-320 °K)

Sidney B. Lang

Department of Chemical Engineering, McGill University, Montreal 101, *Quebec, Canada*

(Received 12 October 1970)

The pyroelectric coefficient (at constant stress) of lithium sulfate monohydrate was measured over the temperature range 4.2–320°K, in order to resolve a discrepancy between the results of Ackermann and those of Gladkii and Zheludev, and to extend the data to below 88 °K. The pyroelectric coefficient was observed to change sign at 106 °K in agreement with the results of Gladkii and Zheludev. The coefficient passed through a broad extremum at 50 °K and approached zero at 4.2 °K. The primary and secondary pyroelectric coefficients were calculated over the temperature range; their cancellation at 106 °K causes the sign change in the pyroelectric coefficient at constant stress. The secondary coefficient is positive at all temperatures, but the primary coefficient changes sign at 158 °K. The Born lattice-dynamical theory of the primary pyroelectric effect was extended to include contributions due both to the acoustical and to the optical spectra of a material. A Debye temperature and five Einstein temperatures calculated from heat-capacity data were used to derive an analytical expression for the primary pyroelectric coefficient.

INTRODUCTION

The first measurements of the pyroelectric coefficient of lithium sulfate monohydrate (LSM) were published by Ackermann in 1915.[1] He determined the pyroelectric coefficient (at constant stress) at discrete temperature values between 23 and 352 °K, using a static technique. He found that the coefficient increased montonically with increasing temperature, with no change in sign at any temperature. Recently Gladkii and Zheludev[2] repeated the measurements down to 88 °K, observing an anomalous change in sign at about 110 °K. To resolve the discrepancy, we repeated the measurements, extending the temperature range down to 4.2 °K in order to observe the very-low-temperature behavior of the pyroelectric coefficient. The measurements reported here are the first continuous ones over a broad temperature range ever determined on a pyroelectric but nonferroelectric material. Using published piezoelectric, elastic, thermal-expansion, and heat-capacity data, the pyroelectric coefficients were resolved into the primary and secondary components. An expression for the primary pyroelectric coefficient was derived by means of an extension of the Born lattice-dynamics theory of pyroelectricity.

LSM is a monoclinic crystal, point group 2, with the lattice parameters[3] $a=8.18$ Å, $b=4.87$ Å, $c=5.45$ Å, and $\beta=107.3°$. Bechmann[4] has published piezoelectric and elastic compliance constants referred to a set of axes in which z is colinear with a, x lies in the obtuse angle between a and c, and y is parallel to b, but is directed so as to make a left-handed set of coordinates with x and z. Although this usage is not strictly according to the IRE convention,[5] Bechmann's system has been adopted in the literature[6] and it will be used here. Calculations described later in this report utilized the elastic compliance coefficients (s), the piezoelectric stress coefficients (d), their temperature dependencies, and the thermal-expansion coefficients (α). These coefficients, corresponding to the coordinate system described above, were calculated from the original references.[3,7] There were a few minor discrepancies between some calculated values and those reported in Landolt-Börnstein,[4] the differences probably being the result of round-off errors.

EXPERIMENTAL METHOD AND RESULTS

The pyroelectric coefficient was determined at constant stress using the dynamic technique of Lang and Steckel.[8] In this method, the coefficient is calculated from the pyroelectric voltage produced as the temperature of the material under study is